

This discussion paper is/has been under review for the journal Atmospheric Chemistry and Physics (ACP). Please refer to the corresponding final paper in ACP if available.

# Understanding isoprene photo-oxidation using observations and modelling over a subtropical forest in the Southeast US

L. Su<sup>1</sup>, E. G. Patton<sup>2</sup>, J. Vilà-Guerau de Arellano<sup>3</sup>, A. B. Guenther<sup>4</sup>, L. Kaser<sup>5</sup>, B. Yuan<sup>6,7</sup>, F. Xiong<sup>8</sup>, P. B. Shepson<sup>8,9</sup>, L. Zhang<sup>10</sup>, D. O. Miller<sup>10</sup>, W. H. Brune<sup>10</sup>, K. Baumann<sup>11</sup>, E. Edgerton<sup>11</sup>, A. Weinheimer<sup>5</sup>, and J. E. Mak<sup>1</sup>

<sup>1</sup>School of Marine and Atmospheric Sciences, Stony Brook University, Stony Brook, NY, USA

<sup>2</sup>Mesoscale and Microscale Meteorology Laboratory, National Center for Atmospheric Research, Boulder, CO, USA

<sup>3</sup>Meteorology and Air Quality Section, Wageningen University and Research Center, Wageningen, the Netherlands

<sup>4</sup>Department of Earth System Science, University of California, Irvine, CA, USA

<sup>5</sup>Atmospheric Chemistry Observations & Modeling Laboratory, National Center for Atmospheric Research, Boulder, CO, USA

<sup>6</sup>Earth System Research Laboratory, Chemical Sciences Division, National Oceanic and Atmospheric Administration, Boulder, CO, USA

<sup>7</sup>Cooperative Institute for Research in Environmental Sciences, University of Colorado, Boulder, CO, USA

ACPD

15, 31621–31663, 2015

Isoprene  
photo-oxidation in  
the Southeast US

L. Su et al.

[Title Page](#)

[Abstract](#)

[Introduction](#)

[Conclusions](#)

[References](#)

[Tables](#)

[Figures](#)

◀

▶

◀

▶

[Back](#)

[Close](#)

[Full Screen / Esc](#)

[Printer-friendly Version](#)

[Interactive Discussion](#)



<sup>8</sup>Department of Chemistry, Purdue University, West Lafayette, IN, USA

<sup>9</sup>Department of Earth, Atmospheric and Planetary Sciences, Purdue University, West Lafayette, IN, USA

<sup>10</sup>Department of Meteorology, Pennsylvania State University, University Park, PA, USA

<sup>11</sup>Atmospheric Research and Analysis Inc., Cary, NC, USA

Received: 13 October 2015 – Accepted: 2 November 2015 – Published: 11 November 2015

Correspondence to: J. E. Mak (john.mak@stonybrook.edu)

Published by Copernicus Publications on behalf of the European Geosciences Union.

ACPD

15, 31621–31663, 2015

Isoprene  
photo-oxidation in  
the Southeast US

L. Su et al.

[Title Page](#)

[Abstract](#)

[Introduction](#)

[Conclusions](#)

[References](#)

[Tables](#)

[Figures](#)



[Back](#)

[Close](#)

[Full Screen / Esc](#)

[Printer-friendly Version](#)

[Interactive Discussion](#)



## Abstract

The emission, dispersion and photochemistry of isoprene ( $C_5H_8$ ) and related chemical species in the convective boundary layer (CBL) during sunlit daytime was studied over a mixed forest in the Southeast United States by combining ground-based and aircraft observations. Fluxes of isoprene and monoterpenes were quantified at the top of the forest canopy using a high resolution Proton Transfer Reaction Time of Flight Mass Spectrometer (PTR-TOF-MS). Snapshot (~2 min sampling duration) vertical profiles of isoprene, methyl vinyl ketone (MVK) + methacrolein (MACR), and monoterpenes were collected from aircraft every hour in the CBL (100–1000 m). Both ground-based and airborne collected volatile organic compound (VOC) data are used to constrain the initial conditions of a mixed layer chemistry model (MXLCH), which is applied to examine the chemical evolution of the  $O_3$ - $NO_x$ - $HO_x$ -VOC system and how it is affected by boundary layer dynamics in the CBL. The chemical loss rate of isoprene (~1 h) is similar to the turbulent mixing time scale (0.1–0.5 h), which indicates that isoprene concentrations are equally dependent on both photo-oxidation and boundary layer dynamics. Analysis of a model-derived concentration budget suggests that diurnal evolution of isoprene inside the CBL is mainly controlled by surface emissions and chemical loss. The NO to  $HO_2$  ratio (NO :  $HO_2$ ) is used as an indicator of anthropogenic impact on the CBL chemical composition, and spans a wide range (1–163). The fate of hydroxyl-substituted isoprene peroxy radical ( $HOC_5H_8OO^\cdot$ ; ISOPOO) is strongly affected by NO :  $HO_2$ , shifting from NO-dominant to NO- $HO_2$ -balanced condition from early morning to noontime. This chemical regime change is reflected in the diurnal evolution of isoprene hydroxynitrates (ISOPN) and isoprene hydroperoxides (ISOPOOH).

## 1 Introduction

Isoprene ( $C_5H_8$ ) from biogenic emissions is the most abundant non-methane volatile organic compound (VOC) in the atmosphere (Guenther et al., 1995). Once emitted, the

[Title Page](#)[Abstract](#)[Introduction](#)[Conclusions](#)[References](#)[Tables](#)[Figures](#)[|◀](#)[▶|](#)[◀](#)[▶](#)[Back](#)[Close](#)[Full Screen / Esc](#)[Printer-friendly Version](#)[Interactive Discussion](#)

distribution of isoprene within the convective CBL is controlled via both photochemical oxidation and turbulent mixing. VOC emissions from forests have been studied extensively for more than 20 years (Guenther et al., 1991). More recent work has expanded the focus from emissions to impacts on regional forest chemistry (Kim et al., 2010; Karl et al., 2013; Park et al., 2013). These advances have exposed large uncertainties and unknown mechanisms in both chemistry and dynamics.

Isoprene chemistry over tropical forests has also been studied due to its influence on tropospheric chemistry through high emission (Karl et al., 2007) and proposed impact on OH recycling mechanisms under low- $\text{NO}_x$  condition (Lelieveld et al., 2008; Whalley et al., 2011). Isoprene oxidation is usually initiated by addition of an OH to one of the C=C double bonds followed by fast reaction with  $\text{O}_2$ . Six isomeric hydroxyl-substituted isoprene peroxy radicals ( $\text{HOCH}_2\text{CH}_2\text{OO}^\bullet$ ; ISOPOO) are then produced. Large uncertainties arise in the subsequent reactions of ISOPOO radicals (Orlando and Tyndall, 2012). In pristine tropical forest areas, the  $\text{HO}_2$  pathway likely dominates (Paulot et al., 2009). Other reactions include self- and cross-reactions with organic peroxy radicals ( $\text{RO}_2$ ) and unimolecular isomerization (Peeters and Muller, 2010; Crounse et al., 2011).

Under NO-dominant conditions, ISOPOO mainly reacts with NO to produce  $\text{NO}_2$ , methyl vinyl ketone (MVK), and methacrolein (MACR). In urban environments where anthropogenic emissions of  $\text{NO}_x$  and non methane hydrocarbons (NMHC) are high, model outputs generally agree with observations of OH concentration during noon-time (Shirley et al., 2006; Hofzumahaus et al., 2009). However, for urban environments where  $\text{NO}_x$  mixing ratios vary by several orders of magnitude, model simulation outputs still underestimate the observed OH under low NO mixing ratios (< 1 ppbv) (Hofzumahaus et al., 2009; Lu et al., 2012). As a result, additional information on  $\text{HO}_2 \rightarrow \text{OH}$  recycling process is needed to bridge the gap between model outputs and observations.

The term “low- $\text{NO}_x$ ” can introduce ambiguity when interpreting ISOPOO chemistry (Liu et al., 2013). First, the definition for the threshold of “low- $\text{NO}_x$ ” is usually arbitrarily based either on instrument performance or other standards during different laboratory

## Isoprene photo-oxidation in the Southeast US

L. Su et al.

[Title Page](#)

[Abstract](#)

[Introduction](#)

[Conclusions](#)

[References](#)

[Tables](#)

[Figures](#)

◀

▶

[Back](#)

[Close](#)

[Full Screen / Esc](#)

[Printer-friendly Version](#)

[Interactive Discussion](#)



or field experiments. For example, NO mixing ratios below 50 pptv (Lelieveld et al., 2008), 150 pptv (Xie et al., 2013), and 200 pptv (Lu et al., 2012) have all been used to indicate “low- $\text{NO}_x$ ” conditions. Second,  $\text{HO}_2$ ,  $\text{RO}_2$  and their contribution to the fate of ISOPOO radicals are not explicitly represented in the context of low- $\text{NO}_x$  condition. It has been suggested that “NO-dominant” or “ $\text{HO}_2$ -dominant” should be used instead when applying laboratory condition to the atmospheric condition (Liu et al., 2013; Wennberg, 2013). In this study, we use the ratio of NO to  $\text{HO}_2$  ( $\text{NO} : \text{HO}_2$ ) to indicate the anthropogenic influence on ambient air composition and discuss the effect on ISOPOO chemistry under different  $\text{NO} : \text{HO}_2$  values.

While large efforts have been dedicated to the study of reactive VOC chemistry, the temporal and spatial variation of those species in the convective CBL is also affected by the boundary layer dynamics (Kristensen et al., 2010). Regional model simulations are carried out to study the interplay between chemistry and dynamics. Depending on the complexity levels of dynamics representation, models can range from the simple 0-dimension box model without accounting for the fluid dynamics (van Stratum et al., 2012), mixed-layer model (extending 0-dimension model by including the main dynamic processes of the CBL) (de Arellano et al., 2011), 1-dimensional transport model (Gao et al., 1993; Kristensen et al., 2010), to complex large eddy simulation (LES) (Patton et al., 2001). Box models are easy to implement but they are unable to incorporate the influence of the dynamical processes controlling the atmospheric boundary layer's diurnal evolution. LES resolves the turbulence and associated organized structures, but is computationally expensive, especially when coupled with complex chemical schemes. The mixed-layer model represents a useful compromise between a box model and an LES, it is suitable to study both the boundary layer dynamics and  $\text{O}_3\text{-NO}_x\text{-HO}_x\text{-VOC}$  chemistry within the measurement scale of this study, while still maintaining the simplicity of a 0-dimension model (de Arellano et al., 2011).

The Southeast Atmosphere Study (SAS) campaign was carried out during summer 2013 in Alabama. The campaign included comprehensive observations of VOCs and other trace gases (e.g.,  $\text{O}_3$ ,  $\text{NO}_x$ , and  $\text{HO}_x$ ) from airborne and ground-based platforms

## Isoprene photo-oxidation in the Southeast US

L. Su et al.

[Title Page](#)

[Abstract](#)

[Introduction](#)

[Conclusions](#)

[References](#)

[Tables](#)

[Figures](#)

◀

▶

◀

▶

[Back](#)

[Close](#)

[Full Screen / Esc](#)

[Printer-friendly Version](#)

[Interactive Discussion](#)



<a href="#">Title Page</a>	
<a href="#">Abstract</a>	<a href="#">Introduction</a>
<a href="#">Conclusions</a>	<a href="#">References</a>
<a href="#">Tables</a>	<a href="#">Figures</a>
<a href="#">◀</a>	<a href="#">▶</a>
<a href="#">◀</a>	<a href="#">▶</a>
<a href="#">Back</a>	<a href="#">Close</a>
<a href="#">Full Screen / Esc</a>	
<a href="#">Printer-friendly Version</a>	
<a href="#">Interactive Discussion</a>	

(Hidy et al., 2014). In this study, we investigated the photochemistry of isoprene based on both ground-based and airborne observations during the SAS campaign. The experiment layout is shown in Fig. 1, which also includes schematic of the important processes controlling the diurnal evolution of chemical species in the boundary layer.  
5 During the campaign, vertical profiles of VOCs were quantified with airborne sampling and subsequent measurements by using a Proton Transfer Reaction Time of Flight Mass Spectrometer (PTR-TOF-MS). Ground-based eddy covariance (EC) was used to measure VOC fluxes on a tower above the forest canopy. A mixed-layer chemistry model was used to study how different processes (entrainment, boundary layer dynamics,  
10 surface emission, deposition, chemical production and loss) control the evolution of trace gases inside the CBL. SAS observations are used to impose the early morning initial conditions and the surface/free tropospheric boundary conditions. We discuss isoprene photochemistry by focusing on the fate of ISOPOO radicals under different NO : HO<sub>2</sub> values.

## 15 2 Experimental

### 2.1 Field sites

The SAS field campaign was carried out during the summer of 2013 (from 1 June to 15 July) in central Alabama. There were two ground-based sampling sites: one near Marion, AL, at the Alabama Aquatic Biodiversity Centre (32°41'40" N, 87°14'55" W;  
20 hereafter as the AABC site), and the other one was located near Centreville, AL, which is part of the South-Eastern Aerosol Research and Characterization network (32°54'12" N, 87°15'0" W; hereafter as the SEARCH site), situated about 24 km to the north-northwest of the AABC site (Fig. 2). The two sampling sites were located inside mixed forest canopies. The tower based observations described in this manuscript are focused on the AABC site where the average canopy height was ~ 35 m. Eight 100 m step transects conducted in the footprint of the AABC flux tower showed that the forest



was composed of 26 % *Liquidambar styraciflua* (sweetgum), 21 % *Nyssa species* (Tupelos), 16 % *Pinus* species (Pines), 14 % *Quercus* sp. (Oaks), 11 % *Liriodendron* sp. (Tulip-poplars), 9 % *Taxodium* sp. (Baldcypress) and 3 % *Ostrya* sp. (Hophornbeams).

## 2.2 Air sample collection

- 5 Two sets of sampling systems were implemented simultaneously during the SAS campaign. Vertical profiles of air above the forest canopy and inside the CBL (100–1000 m a.s.l.) were collected by using the Whole Air Sample Profiler (WASP) system installed on a model Long-EZ research airplane (hereafter: Long-EZ) (Mak et al., 2013). The WASP system is integrated with a meteorological data monitoring system (the 10 Aircraft-Integrated Meteorological Measurement System (AIMMS-20), Aventech Research Inc.), which was used to measure the ambient temperature, relative humidity (RH), GPS altitude, latitude, longitude, and 3-D wind components. In brief, the WASP system includes a 150 m coiled tubing, which is used to collect the ambient air sample during the aircraft's ascending phase. The altitude of the air samples collected inside 15 the tubing is "marked" by injecting tracer gas (propene,  $C_3H_6$ ) into the air stream at a preset frequency. For detailed description of the principle of the WASP system refer to Sect. 4.2 and (Mak et al., 2013). Flights were carried out during the day (10:00–17:00 Central Standard Time (CST)) when intensive photo-oxidation and turbulent mixing occurred. The time interval for sample collection was ~2 min (Table 1). The aircraft 20 usually started sampling from ~100 m a.g.l. and stopped at ~1000 m (cf. Sect. 5). After each research flight (RF), the WASP tubing was sealed and transported to the AABC site in 30 min, where the air samples inside the tubing were analysed by a high resolution Proton Transfer Reaction Time of Flight Mass Spectrometer (PTR-TOF-MS 8000, Ionicon Analytik GmbH, Austria). A total of 14 RFs were carried out (5 over the 25 SEARCH site and 9 over the AABC site; Table 1) between 1 and 13 June 2013.

VOC eddy covariance (EC) fluxes were measured from the top of the forest canopy at the AABC site between 1 June and 14 July 2013 using the same PTR-TOF-MS. A 3/8 inch outer diameter (OD) perfluoro alkoxy (PFA) tubing (~50 m length, not heated)

<a href="#">Title Page</a>	
<a href="#">Abstract</a>	<a href="#">Introduction</a>
<a href="#">Conclusions</a>	<a href="#">References</a>
<a href="#">Tables</a>	<a href="#">Figures</a>
<a href="#">◀</a>	<a href="#">▶</a>
<a href="#">◀</a>	<a href="#">▶</a>
<a href="#">Back</a>	<a href="#">Close</a>
<a href="#">Full Screen / Esc</a>	
<a href="#">Printer-friendly Version</a>	
<a href="#">Interactive Discussion</a>	



was mounted from the top of the flux tower (44 m) to the field laboratory trailer on the ground level. Sample air flow was  $\sim 30 \text{ L min}^{-1}$ , an aliquot of which was diverted to the PTR-TOF-MS.

## 2.3 Instrumentation

- 5 The PTR-TOF-MS was used for two different measurement purposes during the SAS campaign: (1) quantification of the vertical profiles of speciated VOC mixing ratios above the ground-based sites by measuring air samples collected from the WASP system, (2) measurements of air samples through the EC inlet on top of the AABC flux tower, which are used for subsequent calculation of VOC fluxes. The two measurements overlapped between 1 and 13 June. For the overlapping period, an average of 4 WASP samples were measured each day and each sample took  $\sim 15$  min to analyse. During the gap between two WASP sampling periods, the PTR-TOF-MS was connected to the EC line.

15 The basic principle of PTR-TOF-MS was described in Jordan et al. (2009) and Graus et al. (2010). During the campaign, the PTR-TOF-MS was operated under  $\text{H}_3\text{O}^+$  mode, which uses hydronium ions ( $\text{H}_3\text{O}^+$ ) as the primary reagent ions to ionize VOCs species. The ionization conditions in the drift tube were controlled by setting the drift voltage to 575 V, drift temperature to 70 °C and drift pressure to 2.3 mbar, resulting in an  $E/N$  value of about 120 Td (with  $E$  being the electric field strength, and  $N$  the gas number density; 1 Td =  $10^{-17} \text{ V cm}^2$ ). The integration time was set to 1 and 0.1 s for WASP and EC measurements, respectively. A 1/16 inch OD capillary PEEK inlet ( $\sim 1$  m length) heated to 70 °C was used as a transfer line. For analyses of the WASP samples, the flow rate was set at 500 standard cubic centimeters per minute (sccm). The transfer line was connected to an unheated 1/8 inch OD PFA tubing (1 m length), which was connected to the WASP system outlet. For EC samples, the transfer line was connected to the EC line through an unheated 1/8 inch OD PFA tubing (10 cm length). Standard gas calibrations were performed daily by using a custom built dynamic dilution system. Zero air was produced by pumping ambient air outside of the trailer through a catalytic

<a href="#">Title Page</a>	
<a href="#">Abstract</a>	<a href="#">Introduction</a>
<a href="#">Conclusions</a>	<a href="#">References</a>
<a href="#">Tables</a>	<a href="#">Figures</a>
<a href="#">◀</a>	<a href="#">▶</a>
<a href="#">◀</a>	<a href="#">▶</a>
<a href="#">Back</a>	<a href="#">Close</a>
<a href="#">Full Screen / Esc</a>	
<a href="#">Printer-friendly Version</a>	
<a href="#">Interactive Discussion</a>	



convertor heated to 400 °C (Platinum on Quartz Wool, Shimadzu Scientific Instrument Inc.). Gravimetrically prepared standard gas (Apel & Reimer) was dynamically diluted by the zero air and analysed using the PTR-TOF-MS. Diiodomethane ( $\text{CH}_2\text{I}_2$ , Sigma-Aldrich, USA) was added as an external mass scale calibration source (shown as a fragment  $\text{CH}_2\text{I}^+$  at exact  $m/z = 140.920$  in the spectrum) through headspace permeation. Diiodomethane was stored inside a 1/4 inch OD glass tubing (~5 cm length) with one end melted and sealed. The other end of the glass tubing was connected to the PTR-TOF-MS sampling inlet through a 1/16 inch OD capillary PEEK tubing (~2 cm length) and a reducing union.

## 10 2.4 Other measurements

A suite of additional observations were used to constrain the initial and boundary conditions of the MXLCH model. Airborne measurements of isoprene, MVK+MACR, monoterpenes, other trace gases ( $\text{O}_3$ ,  $\text{NO}_x$ ), photolysis rates, and meteorological data (potential temperature and relative humidity) were collected on 12 June 2013 using the NCAR C-130 aircraft (hereafter: C-130). Ground-based observations from the SEARCH site include trace gas concentrations ( $\text{O}_3$ ,  $\text{NO}_x$ ,  $\text{HO}_x$ ) and boundary layer height measurements. 3-D wind components (at 20 Hz) measured at the top of the AABC flux tower were used for eddy covariance calculations. A list of the observed parameters and the corresponding measurement methods and uncertainties are summarized in Table S1 in the Supplement.

## 3 Mixed layer chemistry model

In this study we focus on the convective atmospheric boundary layer observed during the daytime. The vertical profiles of potential temperature and specific humidity (Fig. S1 in the Supplement) show that the CBL was characterized by well-mixed profiles of these observed dynamic variables. It is therefore reasonable to employ mixed-

<a href="#">Title Page</a>	
<a href="#">Abstract</a>	<a href="#">Introduction</a>
<a href="#">Conclusions</a>	<a href="#">References</a>
<a href="#">Tables</a>	<a href="#">Figures</a>
<a href="#">◀</a>	<a href="#">▶</a>
<a href="#">◀</a>	<a href="#">▶</a>
<a href="#">Back</a>	<a href="#">Close</a>
<a href="#">Full Screen / Esc</a>	
<a href="#">Printer-friendly Version</a>	
<a href="#">Interactive Discussion</a>	



**Isoprene  
photo-oxidation in  
the Southeast US**

L. Su et al.

[Title Page](#)

[Abstract](#)

[Introduction](#)

[Conclusions](#)

[References](#)

[Tables](#)

[Figures](#)



[Back](#)

[Close](#)

[Full Screen / Esc](#)

[Printer-friendly Version](#)

[Interactive Discussion](#)



layer theory to predict the boundary layer's dynamical evolution and most-importantly the boundary layer height. The mixed-layer model we use is called MXLCH; MXLCH is a zero-dimensional spatial model which is described in detail elsewhere (de Arellano et al., 2011; van Stratum et al., 2012). The source code of MXLCH can be accessed at <https://github.com/classmodel/mxlch>. In brief, MXLCH is based on the following assumptions:

1. In daytime CBL, the quantities (e.g., potential temperature, specific humidity, trace gas mixing ratios) are perfectly mixed due to strong turbulent mixing and there is only one bulk value for each quantity throughout the CBL. In addition, the CBL growth depends on the conditions at the entrainment zone and at the free troposphere (FT).
2. The CBL height growth is driven by the surface sensible heat and latent heat fluxes. These two variables were prescribed in the model based on observations.
3. The CBL and the FT are separated by an infinitesimally thin inversion layer. Through this layer there is an entrainment flux that exchanges state variables and reactants following the CBL dynamics.
4. Large-scale meteorological forcings (e.g., subsidence, and advection of heat and moisture) are prescribed to the model as external forcings.
5. MXLCH neglects species segregation that could modify chemical reaction rates. (Ouwersloot et al., 2011). In what follows, we use MXLCH to model the evolution of the CBL and trace-gas chemistry during SAS toward further understanding of the processes controlling photochemistry inside the CBL.

### 3.1 Boundary layer meteorology

The meteorological conditions in MXLCH are constrained by the available observations. To reduce the uncertainties introduced from daily variations, averaged values

of the variables (both meteorological data and  $O_3$ - $NO_x$ - $HO_x$  concentrations) from selected days (5, 6, 8, 10–13 June) were calculated and used as the constraints of the initial boundary conditions in MXLCH (Table 2). The selected days were chosen based on: (1) low cloud coverage (indicated by photosynthetically active radiation (PAR); cf. Fig. S2), (2) consistency of  $O_3$ - $NO_x$ -VOC diurnal profiles, and (3) data availability. The apparent sunrise and sunset occurred at 04:41 and 18:57 CST, respectively, during the study period (1 to 13 June 2013) (<http://www.esrl.noaa.gov/gmd/grad/solcalc/>). The averaged sensible and latent heat fluxes were significantly above zero during 06:00–16:30 CST and 06:00–18:00 CST (cf. Fig. S3), respectively. In this study, we focus on analysing the processes under unstable CBL conditions driven primarily by the sensible heat flux. Hence 06:00–16:30 CST is chosen as the model simulation time interval. During the studied time period, the wind directions at the AABC site were mainly from the South-East, with wind speed below  $2\text{ m s}^{-1}$  for most of the time (Fig. S4).

### 3.2 BVOC fluxes

Isoprene and monoterpenes were the two dominant VOC emissions observed at the top of the forest canopy. MXLCH simulations use imposed emissions of these two VOCs species by the observed EC flux data at the AABC flux tower. The EC data from selected days (listed in Sect. 3.1) were averaged to produce a single diurnal flux evolution, where a sinusoidal function was fit to the observed VOC flux temporal evolution taking sampling time as the independent variable (cf. Fig. S5 and Table 3).

### 3.3 $NO_x$ fluxes

The forest–atmosphere exchange of  $NO_x$  affects the oxidative capacity of the CBL through reactions involved in the  $O_3$ - $NO_x$ - $HO_x$ -VOC system. The study of forest–atmosphere  $NO_x$  exchange during daytime is challenging due to the fast conversion between NO and  $NO_2$  within canopy in the presence of  $O_3$ . Direct measurements using the eddy covariance technique at a site in the Sierra Nevada mountains in California

<a href="#">Title Page</a>	
<a href="#">Abstract</a>	<a href="#">Introduction</a>
<a href="#">Conclusions</a>	<a href="#">References</a>
<a href="#">Tables</a>	<a href="#">Figures</a>
<a href="#">◀</a>	<a href="#">▶</a>
<a href="#">◀</a>	<a href="#">▶</a>
<a href="#">Back</a>	<a href="#">Close</a>
<a href="#">Full Screen / Esc</a>	
<a href="#">Printer-friendly Version</a>	
<a href="#">Interactive Discussion</a>	



(June to July 2009) show a midday  $\text{NO}_x$  flux on the order of 1 to 20 pptv  $\text{m s}^{-1}$ , depending on different conditions (Min et al., 2014).  $\text{NO}_x$  fluxes were downward during 06:00–09:00 and upward during 09:00–15:00 LT.  $\text{NO}_x$  eddy covariance fluxes reported in northern Michigan (July to August 2012) show mean NO and  $\text{NO}_2$  flux peak values of  $-4.0 \text{ pptv m s}^{-1}$  (downward) and  $4.8 \text{ pptv m s}^{-1}$  (upward), respectively (Geddes and Murphy, 2014).

$\text{NO}_x$  eddy covariance flux observations are not available during the SAS campaign. Using the soil temperature (at 4.4 cm depth) measured at the AABC flux tower, the soil NO flux (mean  $\pm 1$  standard deviation) is estimated to be  $38.4 \pm 5.0 \text{ pptv m s}^{-1}$  during the sampling period (1 to 13 June) following the parameterization of Thornton et al. (1997). This algorithm is based on pasture land cover type and the calculated NO flux should be regarded as an upper bound since soil NO flux under forest land cover is lower (Thornton et al., 1997). In MXLCH,  $\text{NO}_x$  flux is prescribed with similar patterns as the observations listed above. NO has downward flux during early morning (06:00–08:00 CST), while  $\text{NO}_2$  shows upward flux during 06:00–16:30 CST, with the same pattern as sensible heat flux. To assess the effect of different  $\text{NO}_x$  flux levels on the CBL photochemistry, we carry out sensitivity simulations with three different  $\text{NO}_x$  flux levels. In the base case, NO and  $\text{NO}_2$  have minimum and maximum fluxes at  $-5$  and  $5 \text{ pptv m s}^{-1}$ , respectively (denoted as  $F_{\text{NO}_x} = \pm 5 \text{ pptv m s}^{-1}$ ). The minimum or maximum flux value is used to produce a flux profile the same way as the BVOCs flux described above. The other two  $\text{NO}_x$  flux levels are  $F_{\text{NO}_x} = \pm 15$ , and  $\pm 30 \text{ pptv m s}^{-1}$ . The sensitivity simulation results are discussed in Sect. 6.2.

### 3.4 Chemistry

Two chemistry schemes are coupled separately to MXLCH. In both chemical schemes, the general chemistry involving  $\text{O}_3\text{-NO}_x\text{-HO}_x$  system is obtained as a subset from Model for Ozone and Related Chemical Tracers (MOZART, version 4) (Emmons et al., 2010). The first chemistry scheme includes a highly-reduced version of MOZART

[Title Page](#)[Abstract](#)[Introduction](#)[Conclusions](#)[References](#)[Tables](#)[Figures](#)[◀](#)[▶](#)[◀](#)[▶](#)[Back](#)[Close](#)[Full Screen / Esc](#)[Printer-friendly Version](#)[Interactive Discussion](#)

chemical mechanism involving reactive VOC species (Table 4, hereafter referred to as reduced scheme) (de Arellano et al., 2011). In the reduced scheme: (1) MVK and MACR are lumped together and considered as one compound, (2) no isoprene nitrate chemistry is implemented, ISOPOO + NO channel recycles NO with 100 % yield of NO<sub>2</sub>, (3) no isomerization channel is implemented for ISOPOO radicals, (4) monoterpene oxidation products do not proceed to further reactions. The second chemistry scheme is a subset from GEOS-Chem v9-02 chemical scheme (Mao et al., 2013), which implements updated isoprene oxidation chemistry (Paulot et al., 2009; Peeters et al., 2009; Peeters and Muller, 2010; Crounse et al., 2011) (cf. Tables S2 and S3, hereafter referred to as the complex scheme). In the complex scheme: (1) the reaction rate of ISOPOO radicals through HO<sub>2</sub> channel is updated to take into account of the size effect of the molecule, (2) the isomerization rate of ISOPOO radicals derived by Crounse et al. (2011) is used, (3) nighttime isoprene chemistry is not implemented, which mainly involves reactions with NO<sub>3</sub> radicals, (4) only the first generation isoprene hydroxynitrates (ISOPN =  $\beta$ -hydroxy isoprene nitrate +  $\delta$ -hydroxy isoprene nitrate) are discussed in this study.

Photolysis rates in the complex scheme are calculated using the NCAR Tropospheric Ultraviolet and Visible (TUV) Radiation Model. The relationship between solar zenith angle (sza) and photolysis rates ( $j$ ) are obtained by performing curve fitting to an empirical function  $j = a \times \exp(b/\cos(\text{sza}))$ , where  $a$  and  $b$  are two parameters obtained through curve fitting (Table S4). Aircraft observations of photolysis rates (from the NCAR C-130 aircraft) over the two ground sites are available during 14 June 2013 around noon. The comparisons between TUV outputs and NCAR C-130 observations show that the differences between the two datasets with respect to the observations are within  $\pm 20\%$  except for three reactions (R09, R19, and R27; cf. Table S4), which range from  $\pm 47$  to  $\pm 53\%$  (cf. Table S4 and Fig. S6).

## Isoprene photo-oxidation in the Southeast US

L. Su et al.

[Title Page](#)

[Abstract](#)

[Introduction](#)

[Conclusions](#)

[References](#)

[Tables](#)

[Figures](#)

◀

▶

◀

▶

[Back](#)

[Close](#)

[Full Screen / Esc](#)

[Printer-friendly Version](#)

[Interactive Discussion](#)



## 4 Data processing

### 4.1 PTR-TOF-MS data processing

The PTR-TOF-MS is capable of recording a full mass scan range (1–300  $m/z$  in this study) with high mass resolution and time resolution while still maintaining sufficient sensitivity. However, such a setup can produce data files of a significant size. For processing the data generated by the PTR-TOF-MS, we developed a customized toolbox (Time-of-Flight INterpreting moDule, ToFIND), which is implemented in MATLAB (R2013b, MathWorks Inc., USA). The main routine consists of four subroutines (cf. Sect. S1 in the Supplement for detailed descriptions):

- 10 a. Peak shape fitting: the signals generated by the PTR-TOF-MS are featured with asymmetric peak shape. A fast fitting algorithm optimized for this application is implemented and used by the following three subroutines.
  - 15 b. Time-of-flight to  $m/z$  conversion: parameters are calculated for each cycle to convert the time-of-flight to corresponding  $m/z$ .
  - 20 c. Peak detection: the high mass resolving power of PTR-TOF-MS enables detection of multiple peaks co-existing in one nominal  $m/z$ . A peak detection algorithm is implemented to automatically find those co-existing peaks.
  - 25 d. Signal integration: the left and right bounds for each peak are defined and the signals within the two bounds are summed up.
- The data output from the ToFIND toolbox (in unit of counts per second (cps)) is then normalized and corrected for duty cycle (resulting in unit of normalized cps (ncps)) (Cappellin et al., 2012). The sensitivities for the target VOCs are calculated by using the standard gas calibration system as described above (cf. Sect. 2.3). The sensitivities (mean  $\pm$ 1 standard deviation) during the whole campaign period for isoprene, MVK+MACR, and monoterpenes are  $8.27 \pm 0.28$ ,  $13.63 \pm 1.44$ , and

[Title Page](#)[Abstract](#)[Introduction](#)[Conclusions](#)[References](#)[Tables](#)[Figures](#)[Back](#)[Close](#)[Full Screen / Esc](#)[Printer-friendly Version](#)[Interactive Discussion](#)

$9.22 \pm 0.91$  ncps ppbv $^{-1}$ , respectively (cf. Fig. S7). The instrumental uncertainties for these 3 VOCs are estimated to be 20 % during this campaign.

## 4.2 WASP data processing

WASP samples were analysed by using the PTR-TOF-MS system and the mixing ratios of target VOC species were calculated by using the method described above. The dataset for each RF contains the mixing ratios of the VOC species aligned with the concurrent raw signal intensities of the tracer gas ( $C_3H_6$ , propene) (Mak et al., 2013). The injection pulses of the tracer gas were recorded separately and integrated into the AIMMS-20 output data. In order to reconstruct the altitude of the VOC mixing ratios, the injection pulse signals were aligned with the corresponding propene peak centers. The time resolution of the GPS altitude data and injection pulses are 0.2 and 10 s, respectively. As a result there are a constant of 50 GPS altitude data points within two adjacent injection pulses. The time resolution for the VOCs data measured by the PTR-TOF-MS is constant at 1 s. However, the number of VOCs data points between two tracer gas peaks are determined by a few factors including the PTR-TOF-MS inlet flow rate (500 sccm), the difference of tubing inner diameters (ID) between the PTR-TOF-MS inlet and the WASP coiled tube, and the diffusion of the tracer gas inside the WASP coiled tube during the transportation time period. Thus the number of VOC data points between two tracer gas peaks is not constant (usually between 42 and 48). To resolve this problem, the GPS altitude data between two adjacent injection pulses were interpolated to generate the same number of data points as the VOC data between two propene peak centers. Then each VOCs data point was assigned a corresponding GPS altitude and the updated dataset for each RF contains the mixing ratios of the VOC species aligned with the corresponding GPS altitude.

<a href="#">Title Page</a>	
<a href="#">Abstract</a>	<a href="#">Introduction</a>
<a href="#">Conclusions</a>	<a href="#">References</a>
<a href="#">Tables</a>	<a href="#">Figures</a>
<a href="#">◀</a>	<a href="#">▶</a>
<a href="#">◀</a>	<a href="#">▶</a>
<a href="#">Back</a>	<a href="#">Close</a>
<a href="#">Full Screen / Esc</a>	
<a href="#">Printer-friendly Version</a>	
<a href="#">Interactive Discussion</a>	



## 5 Observation results

A summary of the spatial and temporal coverage for all RFs, together with the corresponding meteorological data is shown in Table 1. Selected vertical profiles of isoprene, MVK+MACR, and monoterpenes are shown in Fig. 3. During early morning (06:55 CST), the averaged mixing ratio of isoprene throughout the vertical profile was 0.60 ppbv, with slightly higher values towards the top and bottom of the profile. The low mixing ratio of isoprene above the canopy during this early time is caused by (1) lack of solar radiation to fuel the biological production of isoprene, and (2) limited vertical turbulent mixing during the early morning hours due to stratification. The slightly higher isoprene in the residual layer at 1000 m might reflect the residual isoprene left from the previous day and preserved during the night due to the absence of photo-oxidation. The absence of photo-oxidation may also lead to the higher mixing ratios of MVK+MACR at 800–1000 m (Fig. 3b). The mixing ratios of monoterpenes within the nocturnal boundary layer (> 1.00 ppbv) were significantly higher than in the residual layer (~ 0.30 ppbv) (Fig. 3c). These high monoterpene mixing ratios near the surface primarily result from night time emissions which are trapped within the shallow nocturnal boundary layer and lower chemical loss rates.

The vertical profiles of VOC species changed dramatically in air samples collected at 10:06 CST. The mixing ratios of isoprene developed a consistent gradient within the well-mixed CBL, with higher values right above the forest canopy and lower values near the top of the CBL. The mixing ratios of MVK+MACR were relatively uniform throughout the CBL. The different vertical profiles between isoprene and MVK+MACR result from their different chemical lifetime scale relative to the turbulent mixing time scales (cf. Sect. 6.2). The sharp gradient of monoterpenes near the top of the CBL (at 350 m) during early morning (Fig. 3c) is significantly reduced due to enhanced vertical turbulent mixing.

One of the main goals of this study is to analyse different processes affecting the diurnal variation of the VOC species within the CBL. To achieve this, the boundary layer

<a href="#">Title Page</a>	
<a href="#">Abstract</a>	<a href="#">Introduction</a>
<a href="#">Conclusions</a>	<a href="#">References</a>
<a href="#">Tables</a>	<a href="#">Figures</a>
<a href="#">◀</a>	<a href="#">▶</a>
<a href="#">◀</a>	<a href="#">▶</a>
<a href="#">Back</a>	<a href="#">Close</a>
<a href="#">Full Screen / Esc</a>	
<a href="#">Printer-friendly Version</a>	
<a href="#">Interactive Discussion</a>	



<a href="#">Title Page</a>	
<a href="#">Abstract</a>	<a href="#">Introduction</a>
<a href="#">Conclusions</a>	<a href="#">References</a>
<a href="#">Tables</a>	<a href="#">Figures</a>
<a href="#">◀</a>	<a href="#">▶</a>
<a href="#">◀</a>	<a href="#">▶</a>
<a href="#">Back</a>	<a href="#">Close</a>
<a href="#">Full Screen / Esc</a>	
<a href="#">Printer-friendly Version</a>	
<a href="#">Interactive Discussion</a>	



height (BLH) during each WASP RF was obtained from ground-based observations (Fig. 4c), and the mixing ratios within the BLH during the RF for each selected VOC species were averaged to produce a representative mixing ratio of this selected VOC species (Fig. 5g–i). Only one RF was carried out to investigate the VOC mixing ratios in early morning (at 06:55 CST). The rest of the RFs span over the convective daytime (10:00–16:00 CST). The evolution of VOC species inside the CBL in the context of surface emissions, other chemical species (e.g., O<sub>3</sub>, NO<sub>x</sub>, and HO<sub>x</sub>), and boundary layer dynamics is discussed in details in Sect. 6.2.

## 6 Model results and discussion

### 10 6.1 Boundary layer dynamics

MXLCH's ability to reproduce the boundary layer dynamics is essential for predicting the evolution of chemical species. The most important parameter is the BLH, which affects entrainment and turbulent mixing of chemical species inside the CBL. The model outputs of potential temperature, specific humidity, and BLH are shown in Fig. 4. The 15 BLH growth is driven by sensible (H) and latent (LE) heat flux (parameterized based on observations; Fig. S3), and is regulated by subsidence and advection. The observations from the ceilometer and sounding system at the SEARCH site indicate a CBL growth rate of about 280 m h<sup>-1</sup> during 07:00–10:00 CST and 80 m h<sup>-1</sup> during 11:00–16:00 CST. A similar BLH growth rate is achieved with MXLCH (Fig. 4c) by adjusting the subsidence rate and the initial potential temperature difference between the CBL and FT (Table 2). The BLH estimated from sounding data at 09:00 and 15:00 CST agree well with the model output (Fig. 4c). Due to the small potential temperature jump between the CBL and FT, the entrainment of relatively warmer air from the FT and surface heat flux is not sufficient to explain the evolution of potential temperature inside the CBL. Advection of relatively warm air is introduced into the system to match the MXLCH output with the observations on top of the AABC flux tower. The specific hu-

midity starts to increase from the beginning of the model simulation due to the turbulent flux of humid air (Fig. S3), reaching a maximum value of  $18.7 \text{ g kg}^{-1}$  at 08:20 CST, and then gradually drops to  $17.0 \text{ g kg}^{-1}$  at around 15:00 CST; this diurnal variation results from the entrainment of relatively dry air from the FT into the CBL. The averaged potential temperature measured from the NCAR C-130 aircraft on 12 June agrees well with both ground-based observations and model outputs. The averaged specific humidity from the NCAR C-130 aircraft, with a large variability, is smaller than ground observations. In general, the MXLCH satisfactorily represents the boundary layer dynamics during the simulation time period of the day (06:00–16:30 CST), which gives us confidence to carry out further analyses on the two chemistry schemes.

## 6.2 Diurnal variation of chemical species

Comparisons between the two chemistry schemes together with the ground and airborne observations are shown in Fig. 5. The diurnal evolution of the  $\text{O}_3\text{-NO}_x$  system from observations was divided into two phases. During 06:00–12:00 CST,  $\text{NO}_2$  mixing

ratios in the CBL showed a steep decrease with a rate of  $-100 \text{ pptv h}^{-1}$ , which is mainly caused by photolysis. This is accompanied with a rapid increase of  $\text{O}_3$  ( $3 \text{ ppbv h}^{-1}$ ). NO mixing ratios reached a peak value at 200 pptv during 06:00–08:00 CST and gradually decreased to 30 pptv after 12:00 CST. During 12:00–16:00 CST,  $\text{O}_3$ , NO and  $\text{NO}_2$  mixing ratios stayed relatively stable at 30 ppbv, 30 pptv, and 200 pptv, respectively. Airborne  $\text{O}_3$  and  $\text{NO}_x$  mixing ratios (from NCAR C-130) were on the upper and lower bound of the ground-based observations, respectively.  $\text{O}_3$  mixing ratios in both chemistry schemes fall within the uncertainty of the observations (Fig. 5a).  $\text{O}_3$  mixing ratios in the reduced scheme are 5 ppbv higher than the complex scheme during 12:00–16:30 CST, which correlates to its higher  $\text{NO}_2$  mixing ratios. NO mixing ratios in the reduced scheme are overestimated throughout the whole simulation time period (Fig. 5b). One possible cause is that isoprene nitrate chemistry is not implemented in the reduced scheme, and the ISOPOO + NO pathway recycles NO with 100 % yield of  $\text{NO}_2$ , which maintains the elevated NO mixing ratios through photolysis during sunlit

[Title Page](#)

[Abstract](#)

[Introduction](#)

[Conclusions](#)

[References](#)

[Tables](#)

[Figures](#)

◀

▶

◀

▶

[Back](#)

[Close](#)

[Full Screen / Esc](#)

[Printer-friendly Version](#)

[Interactive Discussion](#)



daytime. By implementing updated isoprene nitrate chemical mechanisms, the complex scheme agrees better with the observed NO mixing ratios (Fig. 5b). It should be noted that  $\text{NO}_x$  flux prescribed in the complex scheme ( $F_{\text{NO}_x} = \pm 30 \text{ pptv ms}^{-1}$ ) is different from the reduced scheme ( $F_{\text{NO}_x} = \pm 5 \text{ pptv ms}^{-1}$ ) (Table 3). Applying the base 5  $\text{NO}_x$  flux ( $F_{\text{NO}_x} = \pm 5 \text{ pptv ms}^{-1}$ ) in the complex scheme will reduce the  $\text{NO}_x$  mixing ratios to below 80 pptv after 12:00 CST (Fig. S8), which is less than half of the observed  $\text{NO}_2$  mixing ratio (200 pptv). The photochemical cascade will bring down the  $\text{O}_3$  and OH radicals, leading to higher isoprene mixing ratios than observations during 10:00–16:00 CST (Fig. S8). Applying faster photolysis rates of second generation isoprene 10 nitrate products (mainly methyl vinyl ketone nitrate (MVKN) and methacrolein nitrate (MACRN)) (Muller et al., 2014) does not bring up the  $\text{NO}_2$  mixing ratio significantly (data not shown). Thus in the complex scheme higher  $\text{NO}_2$  flux ( $30 \text{ pptv ms}^{-1}$ ) during noontime is necessary to maintain the  $\text{NO}_2$  level at the presence of isoprene nitrate chemistry.

The reduced scheme overestimates OH radical concentration by 50 % during noontime, though it is still within the uncertainty of the observations. In the complex scheme, modelled OH radical concentrations generally agree well with the observations, except during the early morning (06:00–08:00 CST) when the model output is slightly higher than the observations (Fig. 5d). The higher OH radicals are mainly produced through the  $\text{NO} + \text{HO}_2$  reaction, as fuelled by the NO peak during the same time period. On the other hand,  $\text{HO}_2$  radicals in the complex scheme are higher than in the reduced scheme during 06:00–09:00 CST, which are mainly produced through  $\text{RO}_2 + \text{NO}$  pathways implemented in the complex scheme. Certain  $\text{HO}_2$  loss processes that are not included in this study such as heterogeneous uptake onto aerosol particles (Whalley 20 et al., 2010; Lu et al., 2012) may reduce the  $\text{HO}_2$  concentration and subsequently OH radical concentration.

The mixing ratio of isoprene was less than 1.00 ppbv in the early morning (Fig. 5g). During sunlit daytime (10:00–16:00 CST), the mixing ratios of isoprene within the CBL varied between 1.50 and 4.00 ppbv, with lower mixing ratios during the noontime

<a href="#">Title Page</a>	
<a href="#">Abstract</a>	<a href="#">Introduction</a>
<a href="#">Conclusions</a>	<a href="#">References</a>
<a href="#">Tables</a>	<a href="#">Figures</a>
<a href="#">◀◀</a>	<a href="#">▶▶</a>
<a href="#">◀</a>	<a href="#">▶</a>
<a href="#">Back</a>	<a href="#">Close</a>
<a href="#">Full Screen / Esc</a>	
<a href="#">Printer-friendly Version</a>	
<a href="#">Interactive Discussion</a>	



(13:00 CST). This mirrored the higher mixing ratios of OH radicals during the same time period (Fig. 5d), indicating that the abundance of isoprene in the CBL is mainly controlled by photo-oxidation by OH radicals. As the first generation photo-oxidation product, the mixing ratios of MVK+MACR loosely followed isoprene, with lower values during the early morning and similar mixing ratio range during daytime. The variation of isoprene within each WASP RF was larger than MVK+MACR during the daytime, which is reflected in the standard deviations. This is due to the relatively large gradient of isoprene vertical profiles (Fig. 3a). The large variability in isoprene vertical profile can be attributed to its relatively short chemical lifetime during noontime (1 h), in contrast to MVK+MACR (10 h). The chemical lifetime of isoprene is closer to the turbulent mixing time scale (0.1–0.5 h). Another factor could be the land surface heterogeneity (cf. Fig. 2), which can cause large variability in isoprene vertical profiles through the effect of induced secondary circulations (Ouwersloot et al., 2011). The mixing ratios of monoterpenes showed higher values (1.10 ppbv) during the early morning (cf. Sect. 5) while during 10:00–16:00 CST, its mixing ratios fell between 0.20 and 0.60 ppbv with slightly lower values during noontime. VOC mixing ratios measured from the NCAR C-130 aircraft agree well with the WASP RF (Fig. 5g–i).

For the model outputs, the lowest isoprene concentration between 12:00 and 16:00 CST occurs at 14:00 CST in the complex scheme, which is 1 h later than that predicted by the reduced scheme and that observed (at 13:00 CST). One possible explanation to this difference is that the peak value of the OH radical concentrations in the complex scheme is delayed as compared with the reduced scheme during the noontime. As for MVK+MACR, both chemical schemes produce results within the range of observations. Both schemes represent the lower bound of the observed monoterpenes during 10:00–16:00 CST. The mixing ratios of isoprene, MVK+MACR and monoterpenes are lower in the reduced scheme, which is caused by its higher OH radical concentrations. Isoprene mixing ratio is most sensitive due to its high reactivity with OH radicals ( $k_{C_5H_8+OH} = 1.0 \times 10^{-10} \text{ cm}^3 \text{ molec}^{-1} \text{ s}^{-1}$ ).

[Title Page](#)[Abstract](#)[Introduction](#)[Conclusions](#)[References](#)[Tables](#)[Figures](#)[◀](#)[▶](#)[◀](#)[▶](#)[Back](#)[Close](#)[Full Screen / Esc](#)[Printer-friendly Version](#)[Interactive Discussion](#)

The mixing ratios of observed ISOPN showed a peak value of 90 pptv at 10:00 CST, then gradually decreased to 60 pptv at 14:00 CST and remained relatively stable during 14:00–16:00 CST. The model outputs of ISOPN from the complex scheme generally agree with the observed data. The ISOPN yield in the complex scheme is set at 6 %, which is within the range of the results from the chamber experiments ( $9^{+4}_{-3}\%$ ) carried out at the SEARCH site (Xiong et al., 2015). Sensitivity simulations on two other different ISOPN yields at 9 and 12 % overestimate the ISOPN mixing ratios by 30 and 70 %, respectively at 10:00 CST (Fig. S8).

MXLCH reproduces the evolution of major chemical species within the CBL reasonably well, which provides confidence to carry out further analysis on the individual processes controlling the evolution of those compounds in the CBL. In Sect. 6.3 we discuss the influence of boundary layer dynamics and photochemistry on the evolution of  $O_3$  and isoprene. In Sect. 6.4 we focus on interpretation of the isoprene photochemistry under different NO :  $HO_2$  ratios.

### 6.3 Budget analysis of ozone and isoprene

Applying a bulk budget analysis of  $O_3$  and isoprene to differentiate the impact of emission/deposition, entrainment, and chemical production/loss yields:

$$\frac{\partial \langle S \rangle}{\partial t} = \underbrace{\frac{w' S'_s}{h}}_{\text{dynamics}} - \underbrace{\frac{w' S'_h}{h}}_{\text{Entrainment}} + \underbrace{\frac{S_{\text{prod}}}{\text{chemistry}} - \frac{S_{\text{loss}}}{\text{chemistry}}}_{\text{Chemical production - Chemical loss}} \quad (1)$$

where  $\langle S \rangle$  is the mixed-layer mixing ratio of chemical species  $S$  (ppbv);  $h$  is the BLH (m);  $t$  is time (s).

The total tendency of isoprene is largely controlled by emission and chemical loss. The emission tendency peaks at 08:50 CST, while the isoprene flux data peaks at 12:00 CST (Fig. S5). This difference is caused by the BLH evolution (Eq. 1). The chem-

<a href="#">Title Page</a>	<a href="#">Abstract</a>	<a href="#">Introduction</a>
<a href="#">Conclusions</a>	<a href="#">References</a>	
<a href="#">Tables</a>	<a href="#">Figures</a>	
<a href="#">◀</a>	<a href="#">▶</a>	
<a href="#">◀</a>	<a href="#">▶</a>	
<a href="#">Back</a>	<a href="#">Close</a>	
<a href="#">Full Screen / Esc</a>		
	<a href="#">Printer-friendly Version</a>	
	<a href="#">Interactive Discussion</a>	



Isoprene  
photo-oxidation in  
the Southeast US

L. Su et al.

Title Page

Abstract

Introduction

Conclusions

References

Tables

Figures

◀

▶

◀

▶

Back

Close

Full Screen / Esc

Printer-friendly Version

Interactive Discussion



<a href="#">Title Page</a>	
<a href="#">Abstract</a>	<a href="#">Introduction</a>
<a href="#">Conclusions</a>	<a href="#">References</a>
<a href="#">Tables</a>	<a href="#">Figures</a>
<a href="#">◀</a>	<a href="#">▶</a>
<a href="#">◀</a>	<a href="#">▶</a>
<a href="#">Back</a>	<a href="#">Close</a>
<a href="#">Full Screen / Esc</a>	
<a href="#">Printer-friendly Version</a>	
<a href="#">Interactive Discussion</a>	



angle. During noontime, increased  $O_3$  photolysis induces a decrease in the chemical tendency, although the net value is still positive. The surface deposition tendency of  $O_3$  is of comparable magnitude as the chemical tendency. The total  $O_3$  tendency remains positive during 07:00–13:00 CST, reaching a peak value at 09:00 CST.

## 5 6.4 Photochemistry under different NO : HO<sub>2</sub>

In Sect. 6.2, the model results show a wide range NO and HO<sub>2</sub> mixing ratios across the diurnal cycle (Fig. 5), which have varied impacts on the photochemistry inside the CBL. Here we use the ratio of NO to HO<sub>2</sub> (NO : HO<sub>2</sub>, both in units of ppbv) as an indicator of the “cleanliness” of the CBL and analyse the fate of isoprene and its photo-oxidation products under periods with different NO : HO<sub>2</sub> ratios. During the model simulation period (06:00–16:30 CST), NO and HO<sub>2</sub> concentrations vary in the range of 0.028–0.28 ppbv and 0.0018–0.030 ppbv, respectively. The resulting NO : HO<sub>2</sub> ratio ranges from NO-dominant (NO : HO<sub>2</sub> = 163) to NO-HO<sub>2</sub>-balanced (NO : HO<sub>2</sub> = 1) air conditions. Reaction with OH radicals is the major sink of isoprene due to its fast reaction rate with OH radicals under the observed meteorological conditions ( $k_{C_5H_8+OH} = 1.0 \times 10^{-10} \text{ cm}^3 \text{ molec}^{-1} \text{ s}^{-1}$ ). Once emitted into the CBL, isoprene is rapidly oxidized through OH radical addition and subsequent reaction with O<sub>2</sub>, producing a series of isomeric hydroxyl-substituted alkyl peroxy radicals (HOC<sub>5</sub>H<sub>8</sub>OO<sup>•</sup>; ISOPOO). ISOPOO radicals go through several different pathways including reactions with NO, HO<sub>2</sub>, RO<sub>2</sub>, as well as isomerization (Table S3). The branching ratio of each pathway is strongly affected by NO and HO<sub>2</sub> mixing ratios.

The contribution from each reaction pathway listed above is plotted as a function of NO : HO<sub>2</sub> and the results are shown in Fig. 7. The NO pathway represents the major sink of ISOPOO radicals (> 85 %) under a wide range of NO : HO<sub>2</sub> (20–163). After NO : HO<sub>2</sub> falls below 20, the contribution from HO<sub>2</sub> pathway increases dramatically and reaches 54 % at NO : HO<sub>2</sub> = 1, while NO, isomerization, and CH<sub>3</sub>(O)OO<sup>•</sup> pathway constitutes 31, 11, and 3 %, respectively. For the RO<sub>2</sub> pathway, CH<sub>3</sub>(O)OO<sup>•</sup> radical is the

dominant candidate, and yet its contribution is negligible compared to the other reaction pathways throughout the whole NO : HO<sub>2</sub> range. The share of the NO pathway reaches 93 % under large NO : HO<sub>2</sub>, while HO<sub>2</sub> and isomerization each contributes 3 and 4 %, respectively.

With a box model simulation using MCM v3.2 constrained by chamber experiments, Liu et al. (2013) calculated the contributions from NO, HO<sub>2</sub>, and isomerization pathways to be 93, 6, and 0.9 % under NO : HO<sub>2</sub> = 32. These results generally agree with this study under the same NO : HO<sub>2</sub> value (88, 7, and 4 %, respectively). The low end of NO : HO<sub>2</sub> in Liu et al. (2013) (< 1) is out of the range of our model results.

ISOPN and ISOPOOH are the two tracers of isoprene photo-oxidation under NO- and HO<sub>2</sub>-dominant conditions. The diurnal evolution of these two compounds together with NO : HO<sub>2</sub> and isoprene mixing ratios are shown in Fig. 8. The rapid increase of ISOPN mixing ratios (0.032 ppbv h<sup>-1</sup>) during 06:00–09:00 CST coincides with the NO peak during the same time period (0.10–0.28 ppbv, Fig. 5b). The NO : HO<sub>2</sub> ratio spans a large range (5–160) during this time period, which corresponds to 66–93 % sink of ISOPOO radicals through the NO pathway (Fig. 7). Under this NO-dominant air condition, the ISOPN mixing ratios are mainly constrained by the availability of isoprene during this time period, which is reflected by the high correlation between these two species. After 09:00 CST, the NO : HO<sub>2</sub> falls below 5 and stays at ~ 1 during 12:00–16:00 CST. The ISOPN mixing ratios start to decrease even though the isoprene (3–4 ppbv) is still abundant in the CBL. This is due to the shift from NO-dominant to NO-HO<sub>2</sub>-balanced conditions, and ISOPN production becomes constrained by NO availability. Meanwhile, ISOPN is relatively short lived (chemical lifetime 2 h) under the OH radical concentration of ~ 1.5 × 10<sup>6</sup> molec cm<sup>-3</sup>.

The mixing ratio of ISOPOOH shows reversed correlation with NO : HO<sub>2</sub>. Its mixing ratio starts to rise after 07:00 CST and reaches 1.5 ppbv at 16:00 CST. The higher mixing ratio of ISOPOOH during the end of the model simulation is a result of (1) sufficient isoprene and HO<sub>2</sub> radicals, and (2) longer chemical life time of ISOPOOH (5 h) due to reduced OH radicals in the CBL. The peak value of ISOPOOH mixing ratio predicted

<a href="#">Title Page</a>	
<a href="#">Abstract</a>	<a href="#">Introduction</a>
<a href="#">Conclusions</a>	<a href="#">References</a>
<a href="#">Tables</a>	<a href="#">Figures</a>
<a href="#">◀</a>	<a href="#">▶</a>
<a href="#">◀</a>	<a href="#">▶</a>
<a href="#">Back</a>	<a href="#">Close</a>
<a href="#">Full Screen / Esc</a>	
<a href="#">Printer-friendly Version</a>	
<a href="#">Interactive Discussion</a>	



by MXLCH (1.5 ppbv) is significantly higher than ground-based observations at the SEARCH site (0.40 ppbv, measured on 8 June 2013) (Nguyen et al., 2015). The dry deposition velocity of ISOOPOH in MXLCH is set to  $2.5 \text{ cm s}^{-1}$ , which is adopted from the same ground-based observation at the SEARCH site (Nguyen et al., 2015). One possible explanation of the large discrepancy between model output and observation is the partitioning of ISOOPOH to aerosol phase due to its lower vapour pressure and potentially high condensed phase reactivity (Rivera-Rios et al., 2014). Unfortunately the aerosol-gas phase chemistry is not implemented in this study for simplicity. Future work should incorporate an aerosol phase module into MXLCH. Despite the higher ISOOPOH mixing ratios from MXLCH, the averaged value of ISOOPOH/ISOPN values from MXLCH (13; both species are in units of ppbv) is within the range of the GEOS-Chem model outputs for time period of August 2013 over the Southeast US (5–15) (Kim et al., 2015).

## 7 Conclusions

The WASP system enabled us to quantify the vertical profiles of VOC species inside the CBL at high temporal (hourly) resolution. Before sunrise, isoprene and MVK+MACR exhibit lower mixing ratios (< 1.00 ppbv) within and above the CBL. This is due to the absence of solar radiation, which drives biological isoprene production, and convective turbulent mixing. Monoterpenes, on the other hand, have a large contrast in mixing ratios within and above the CBL in early morning. This is largely attributed to night-time emissions and lack of vertical turbulent mixing, trapping the monoterpenes within the nocturnal boundary layer's limited depth. During sunlit noontime, observed vertical profiles of isoprene and monoterpenes reveal a vertical gradient within the CBL, with higher mixing ratios near the forest canopy and low values towards the top of the CBL.

The MXLCH model generally reproduces the boundary layer's diurnal evolution (e.g., BLH growth, potential temperature, and specific humidity). Accurate modelling of BLH is essential for investigating trace gas photochemistry in that the FT-CBL exchange

## Isoprene photo-oxidation in the Southeast US

L. Su et al.

[Title Page](#)

[Abstract](#)

[Introduction](#)

[Conclusions](#)

[References](#)

[Tables](#)

[Figures](#)

◀

▶

◀

▶

[Back](#)

[Close](#)

[Full Screen / Esc](#)

[Printer-friendly Version](#)

[Interactive Discussion](#)



plays an important role in regulating the vertical distribution and evolution of trace gas species in the CBL through entrainment.

Isoprene photochemistry is strongly influenced by NO : HO<sub>2</sub> values. This is reflected through the fate of ISOPOO radicals, which shift from a NO-dominant pathway (with a contribution of 93 %) to a NO-HO<sub>2</sub>-balanced pathway (with a contribution of 54 %) from early morning (NO : HO<sub>2</sub> = 163) to noontime (NO : HO<sub>2</sub> = 1). As a result, ISOPN and ISOPOOH show peaks during 09:00 and 16:00 CST, respectively. ISOPN production is constrained by isoprene before 09:00 CST. The mixing ratio of ISOPN decreases after 09:00 CST due to its short lifetime (2 h) and limited NO availability. ISOPOOH is inversely correlated with NO : HO<sub>2</sub>. Model outputs significantly overestimate ISOPOOH mixing ratios in the late afternoon when comparing with ground-based observation, with implications for gas to aerosol partitioning of ISOPOOH.

The Supplement related to this article is available online at  
doi:10.5194/acpd-15-31621-2015-supplement.

Acknowledgements. We thank the organizers of the SAS study. We especially thank Andrew Turnipseed for providing VOC standard gas during the campaign and Bill Hansen from Vaiden Field Airport for logistics. We would like to acknowledge operational, technical and scientific support provided by NCAR's Earth Observing Laboratory, sponsored by the National Science Foundation. This study is supported by US Environmental Protection Agency (EPA) STAR program grant 1110369, NSF atmospheric chemistry program, and UltraPure Air, LLC. E. G. Patton was supported by NCAR's Bio-hydro-atmosphere interactions of Energy, Aerosols, Carbon, H<sub>2</sub>O, Organics and Nitrogen (BEACHON) project.

ACPD

15, 31621–31663, 2015

## Isoprene photo-oxidation in the Southeast US

L. Su et al.

[Title Page](#)

[Abstract](#)

[Introduction](#)

[Conclusions](#)

[References](#)

[Tables](#)

[Figures](#)

◀

▶

◀

▶

[Back](#)

[Close](#)

[Full Screen / Esc](#)

[Printer-friendly Version](#)

[Interactive Discussion](#)



## References

- Cappellin, L., Karl, T., Probst, M., Ismailova, O., Winkler, P. M., Soukoulis, C., Aprea, E., Mark, T. D., Gasperi, F., and Biasioli, F.: On quantitative determination of volatile organic compound concentrations using proton transfer reaction time-of-flight mass spectrometry, Environ. Sci. Technol., 46, 2283–2290, 2012. 31634
- Crounse, J. D., Paulot, F., Kjaergaard, H. G., and Wennberg, P. O.: Peroxy radical isomerization in the oxidation of isoprene, Phys. Chem. Chem. Phys., 13, 13607–13613, doi:10.1039/C1cp21330j, 2011. 31624, 31633
- de Arellano, J. V. G., Patton, E. G., Karl, T., van den Dries, K., Barth, M. C., and Orlando, J. J.: The role of boundary layer dynamics on the diurnal evolution of isoprene and the hydroxyl radical over tropical forests, J. Geophys. Res.-Atmos., 116, D07304, doi:10.1029/2010JD014857, 2011. 31625, 31630, 31633
- Emmons, L. K., Walters, S., Hess, P. G., Lamarque, J.-F., Pfister, G. G., Fillmore, D., Granier, C., Guenther, A., Kinnison, D., Laepple, T., Orlando, J., Tie, X., Tyndall, G., Wiedinmyer, C., Baughcum, S. L., and Kloster, S.: Description and evaluation of the model for ozone and related chemical tracers, version 4 (MOZART-4), Geosci. Model Dev., 3, 43–67, doi:10.5194/gmd-3-43-2010, 2010. 31632
- Gao, W., Wesely, M. L., and Doskey, P. V.: Numerical modeling of the turbulent-diffusion and chemistry of NO<sub>x</sub>, O<sub>3</sub>, isoprene, and other reactive trace gases in and above a forest canopy, J. Geophys. Res.-Atmos., 98, 18339–18353, 1993. 31625
- Geddes, J. A. and Murphy, J. G.: Observations of reactive nitrogen oxide fluxes by eddy covariance above two midlatitude North American mixed hardwood forests, Atmos. Chem. Phys., 14, 2939–2957, doi:10.5194/acp-14-2939-2014, 2014. 31632
- Graus, M., Muller, M., and Hansel, A.: High Resolution PTR-TOF: Quantification and formula confirmation of VOC in real time, J. Am. Soc. Mass Spectr., 21, 1037–1044, 2010. 31628
- Guenther, A., Hewitt, C. N., Erickson, D., Fall, R., Geron, C., Graedel, T., Harley, P., Klinger, L., Lerdau, M., Mckay, W. A., Pierce, T., Scholes, B., Steinbrecher, R., Tallamraju, R., Taylor, J., and Zimmerman, P.: A global-model of natural volatile organic-compound emissions, J. Geophys. Res.-Atmos., 100, 8873–8892, 1995. 31623, 31642
- Guenther, A. B., Monson, R. K., and Fall, R.: Isoprene and monoterpene emission rate variability – observations with eucalyptus and emission rate algorithm development, J. Geophys. Res.-Atmos., 96, 10799–10808, 1991. 31624

Title Page

Abstract

Introduction

Conclusions

References

Tables

Figures

◀

▶

◀

▶

Back

Close

Full Screen / Esc

Printer-friendly Version

Interactive Discussion



## Isoprene photo-oxidation in the Southeast US

L. Su et al.

<a href="#">Title Page</a>	
<a href="#">Abstract</a>	<a href="#">Introduction</a>
<a href="#">Conclusions</a>	<a href="#">References</a>
<a href="#">Tables</a>	<a href="#">Figures</a>
<a href="#">◀</a>	<a href="#">▶</a>
<a href="#">◀</a>	<a href="#">▶</a>
<a href="#">Back</a>	<a href="#">Close</a>
<a href="#">Full Screen / Esc</a>	
<a href="#">Printer-friendly Version</a>	
<a href="#">Interactive Discussion</a>	



- Hidy, G. M., Blanchard, C. L., Baumann, K., Edgerton, E., Tanenbaum, S., Shaw, S., Knipping, E., Tombach, I., Jansen, J., and Walters, J.: Chemical climatology of the southeastern United States, 1999–2013, *Atmos. Chem. Phys.*, 14, 11893–11914, doi:10.5194/acp-14-11893-2014, 2014. 31626
- Hofzumahaus, A., Rohrer, F., Lu, K. D., Bohn, B., Brauers, T., Chang, C. C., Fuchs, H., Holland, F., Kita, K., Kondo, Y., Li, X., Lou, S. R., Shao, M., Zeng, L. M., Wahner, A., and Zhang, Y. H.: Amplified trace gas removal in the troposphere, *Science*, 324, 1702–1704, 2009. 31624
- Jordan, A., Haidacher, S., Hanel, G., Hartungen, E., Mark, L., Seehauser, H., Schottkowsky, R., Sulzer, P., and Mark, T. D.: A high resolution and high sensitivity proton-transfer-reaction time-of-flight mass spectrometer (PTR-TOF-MS), *Int. J. Mass Spectrom.*, 286, 122–128, 2009. 31628
- Karl, T., Guenther, A., Yokelson, R. J., Greenberg, J., Potosnak, M., Blake, D. R., and Artaxo, P.: The tropical forest and fire emissions experiment: emission, chemistry, and transport of biogenic volatile organic compounds in the lower atmosphere over Amazonia, *J. Geophys. Res.-Atmos.*, 112, D18302, doi:10.1029/2007JD008539, 2007. 31624
- Karl, T., Misztal, P. K., Jonsson, H. H., Shertz, S., Goldstein, A. H., and Guenther, A. B.: Airborne flux measurements of BVOCs above Californian oak forests: experimental investigation of surface and entrainment Fluxes, OH densities, and Damköhler numbers, *J. Atmos. Sci.*, 70, 3277–3287, doi:10.1175/Jas-D-13-054.1, 2013. 31624
- Kim, P. S., Jacob, D. J., Fisher, J. A., Travis, K., Yu, K., Zhu, L., Yantosca, R. M., Sulprizio, M. P., Jimenez, J. L., Campuzano-Jost, P., Froyd, K. D., Liao, J., Hair, J. W., Fenn, M. A., Butler, C. F., Wagner, N. L., Gordon, T. D., Welti, A., Wennberg, P. O., Crounse, J. D., St. Clair, J. M., Teng, A. P., Millet, D. B., Schwarz, J. P., Markovic, M. Z., and Perring, A. E.: Sources, seasonality, and trends of southeast US aerosol: an integrated analysis of surface, aircraft, and satellite observations with the GEOS-Chem chemical transport model, *Atmos. Chem. Phys.*, 15, 10411–10433, doi:10.5194/acp-15-10411-2015, 2015. 31645
- Kim, S., Karl, T., Guenther, A., Tyndall, G., Orlando, J., Harley, P., Rasmussen, R., and Apel, E.: Emissions and ambient distributions of Biogenic Volatile Organic Compounds (BVOC) in a ponderosa pine ecosystem: interpretation of PTR-MS mass spectra, *Atmos. Chem. Phys.*, 10, 1759–1771, doi:10.5194/acp-10-1759-2010, 2010. 31624

## Isoprene photo-oxidation in the Southeast US

L. Su et al.

[Title Page](#)

[Abstract](#)

[Introduction](#)

[Conclusions](#)

[References](#)

[Tables](#)

[Figures](#)

◀

▶

◀

▶

[Back](#)

[Close](#)

[Full Screen / Esc](#)

[Printer-friendly Version](#)

[Interactive Discussion](#)



Kristensen, L., Lenschow, D. H., Gurarie, D., and Jensen, N. O.: A simple model for the vertical transport of reactive species in the convective atmospheric boundary layer, *Bound.-Lay. Meteorol.*, 134, 195–221, doi:10.1007/s10546-009-9443-x, 2010. 31625

Lelieveld, J., Butler, T. M., Crowley, J. N., Dillon, T. J., Fischer, H., Ganzeveld, L., Harder, H., Lawrence, M. G., Martinez, M., Taraborrelli, D., and Williams, J.: Atmospheric oxidation capacity sustained by a tropical forest, *Nature*, 452, 737–740, 2008. 31624, 31625

Liu, Y. J., Herdlinger-Blatt, I., McKinney, K. A., and Martin, S. T.: Production of methyl vinyl ketone and methacrolein via the hydroperoxyl pathway of isoprene oxidation, *Atmos. Chem. Phys.*, 13, 5715–5730, doi:10.5194/acp-13-5715-2013, 2013. 31624, 31625, 31644

Lu, K. D., Rohrer, F., Holland, F., Fuchs, H., Bohn, B., Brauers, T., Chang, C. C., Häseler, R., Hu, M., Kita, K., Kondo, Y., Li, X., Lou, S. R., Nehr, S., Shao, M., Zeng, L. M., Wahner, A., Zhang, Y. H., and Hofzumahaus, A.: Observation and modelling of OH and HO<sub>2</sub> concentrations in the Pearl River Delta 2006: a missing OH source in a VOC rich atmosphere, *Atmos. Chem. Phys.*, 12, 1541–1569, doi:10.5194/acp-12-1541-2012, 2012. 31624, 31625, 31639

Mak, J. E., Su, L., Guenther, A., and Karl, T.: A novel Whole Air Sample Profiler (WASP) for the quantification of volatile organic compounds in the boundary layer, *Atmos. Meas. Tech.*, 6, 2703–2712, doi:10.5194/amt-6-2703-2013, 2013. 31627, 31635

Mao, J. Q., Paulot, F., Jacob, D. J., Cohen, R. C., Crounse, J. D., Wennberg, P. O., Keller, C. A., Hudman, R. C., Barkley, M. P., and Horowitz, L. W.: Ozone and organic nitrates over the eastern United States: sensitivity to isoprene chemistry, *J. Geophys. Res.-Atmos.*, 118, 11256–11268, doi:10.1002/jgrd.50817, 2013. 31633

Min, K.-E., Pusede, S. E., Browne, E. C., LaFranchi, B. W., and Cohen, R. C.: Eddy covariance fluxes and vertical concentration gradient measurements of NO and NO<sub>2</sub> over a ponderosa pine ecosystem: observational evidence for within-canopy chemical removal of NO<sub>x</sub>, *Atmos. Chem. Phys.*, 14, 5495–5512, doi:10.5194/acp-14-5495-2014, 2014. 31632

Nguyen, T. B., Crounse, J. D., Teng, A. P., Clair, J. M. S., Paulot, F., Wolfe, G. M., and Wennberg, P. O.: Rapid deposition of oxidized biogenic compounds to a temperate forest, *P. Natl. Acad. Sci. USA*, 112, E392–E401, doi:10.1073/pnas.1418702112, 2015. 31645

Orlando, J. J. and Tyndall, G. S.: Laboratory studies of organic peroxy radical chemistry: an overview with emphasis on recent issues of atmospheric significance, *Chem. Soc. Rev.*, 41, 6294–6317, 2012. 31624

Ouwersloot, H. G., Vilà-Guerau de Arellano, J., van Heerwaarden, C. C., Ganzeveld, L. N., Krol, M. C., and Lelieveld, J.: On the segregation of chemical species in a clear bound-

ary layer over heterogeneous land surfaces, *Atmos. Chem. Phys.*, 11, 10681–10704, doi:10.5194/acp-11-10681-2011, 2011. 31630, 31640

Park, J.-H., Goldstein, A. H., Timkovsky, J., Fares, S., Weber, R., Karlík, J., and Holzinger, R.: Eddy covariance emission and deposition flux measurements using proton transfer reaction – time of flight – mass spectrometry (PTR-TOF-MS): comparison with PTR-MS measured vertical gradients and fluxes, *Atmos. Chem. Phys.*, 13, 1439–1456, doi:10.5194/acp-13-1439-2013, 2013. 31624

Patton, E. G., Davis, K. J., Barth, M. C., and Sullivan, P. P.: Decaying scalars emitted by a forest canopy: a numerical study, *Bound.-Lay. Meteorol.*, 100, 91–129, 2001. 31625

Paulot, F., Crounse, J. D., Kjaergaard, H. G., Kurten, A., St Clair, J. M., Seinfeld, J. H., and Wennberg, P. O.: Unexpected Epoxide Formation in the Gas-Phase Photooxidation of Isoprene, *Science*, 325, 730–733, 2009. 31633

Peeters, J. and Müller, J. F.: HO<sub>x</sub> radical regeneration in isoprene oxidation via peroxy radical isomerisations. II: experimental evidence and global impact, *Phys. Chem. Chem. Phys.*, 12, 14227–14235, 2010. 31624, 31633

Peeters, J., Nguyen, T. L., and Vereecken, L.: HO<sub>x</sub> radical regeneration in the oxidation of isoprene, *Phys. Chem. Chem. Phys.*, 11, 5935–5939, 2009. 31633

Rivera-Rios, J. C., Nguyen, T. B., Crounse, J. D., Jud, W., St Clair, J. M., Mikoviny, T., Gilman, J. B., Lerner, B. M., Kaiser, J. B., de Gouw, J., Wisthaler, A., Hansel, A., Wennberg, P. O., Seinfeld, J. H., and Keutsch, F. N.: Conversion of hydroperoxides to carbonyls in field and laboratory instrumentation: observational bias in diagnosing pristine versus anthropogenically controlled atmospheric chemistry, *Geophys. Res. Lett.*, 41, 8645–8651, doi:10.1002/2014gl061919, 2014. 31645

Shirley, T. R., Brune, W. H., Ren, X., Mao, J., Lesher, R., Cardenas, B., Volkamer, R., Molina, L. T., Molina, M. J., Lamb, B., Velasco, E., Jobson, T., and Alexander, M.: Atmospheric oxidation in the Mexico City Metropolitan Area (MCMA) during April 2003, *Atmos. Chem. Phys.*, 6, 2753–2765, doi:10.5194/acp-6-2753-2006, 2006. 31624

Thornton, F. C., Pier, P. A., and Valente, R. J.: NO emissions from soils in the southeastern United States, *J. Geophys. Res.-Atmos.*, 102, 21189–21195, doi:10.1029/97jd01567, 1997. 31632

van Stratum, B. J. H., Vilà-Guerau de Arellano, J., Ouwersloot, H. G., van den Dries, K., van Laar, T. W., Martinez, M., Lelieveld, J., Diesch, J.-M., Drewnick, F., Fischer, H., Hosaynali Beygi, Z., Harder, H., Regelin, E., Sinha, V., Adame, J. A., Sörgel, M., Sander, R.,

[Title Page](#)

[Abstract](#)

[Introduction](#)

[Conclusions](#)

[References](#)

[Tables](#)

[Figures](#)

◀

▶

◀

▶

[Back](#)

[Close](#)

[Full Screen / Esc](#)

[Printer-friendly Version](#)

[Interactive Discussion](#)





**Table 1.** Summary of the WASP research flights (RFs). The first four digits in RF no. before the underscore indicate the month and day of the flight, the digit after the underscore indicates the flight number carried out on the specific single day.

RF no.	Site	Latitude	Longitude	Sampling time	Temperature	RH
0601_2	AABC	32.69 to 32.71	−87.26 to −87.24	06:55–06:57	18.9–22.2	0.8–0.9
0605_1	SEARCH	32.90 to 32.91	−87.26 to −87.24	10:05–10:07	21.2–26.2	0.7–0.9
0605_4	AABC	32.69 to 32.71	−87.26 to −87.23	14:23–14:25	22.6–28.2	0.6–0.7
0606_1	SEARCH	32.90 to 32.91	−87.26 to −87.24	10:47–10:49	19.1–24.1	0.7–0.8
0606_3	AABC	32.69 to 32.70	−87.25 to −87.24	14:17–14:19	21.7–25.7	0.7–0.8
0606_5	AABC	32.69 to 32.71	−87.26 to −87.24	16:06–16:09	21.5–27.2	0.7–0.8
0608_3	AABC	32.69 to 32.71	−87.26 to −87.23	12:42–12:44	20.3–25.8	0.6–0.8
0611_1	SEARCH	32.90 to 32.91	−87.26 to −87.24	10:06–10:08	22.6–27.8	0.6–0.8
0611_3	AABC	32.69 to 32.70	−87.25 to −87.24	12:34–12:36	23.2–29.1	0.6–0.7
0611_5	AABC	32.69 to 32.70	−87.25 to −87.23	16:09–16:11	24.2–31.1	0.5–0.7
0612_1	SEARCH	32.90 to 32.91	−87.26 to −87.24	09:51–09:53	22.2–28.5	0.7–0.8
0612_4	SEARCH	32.90 to 32.91	−87.26 to −87.24	15:01–15:03	25.1–31.0	0.5–0.6
0613_2	AABC	32.69 to 32.70	−87.25 to −87.23	11:23–11:25	23.2–29.8	0.6–0.7
0613_4	AABC	32.68 to 32.70	−87.25 to −87.22	14:13–14:15	24.3–31.0	0.5–0.7



**Table 2.** The initial and boundary conditions used in MXLCH.

Parameter	Symbol	Value	Units
Initial BL height	$h$	500 <sup>a</sup>	m
Subsidence rate	$w$	$9.0 \times 10^{-6}$	$\text{m s}^{-1}$
Surface sensible heat flux	$\frac{w' \theta'_s}{w' q'_s}$	$0.10 \sin(\pi t / t_d)$ <sup>b</sup>	$\text{K m s}^{-1}$
Surface latent heat flux	$\frac{w' q'_s}{w' q'_s}$	$0.15 \sin(\pi t / t_d)$ <sup>b</sup>	$\text{g kg}^{-1} \text{ms}^{-1}$
Entrainment/surface heat flux ratio	$\beta = -\frac{w' \theta'_e}{w' \theta'_s}$	0.2	1
Initial BL potential temperature	$\langle \theta \rangle$	296.6 <sup>c</sup>	K
Initial FT potential temperature	$\theta_{FT}$	298.1	K
Potential temperature lapse rate FT	$\gamma_\theta$	0.003	$\text{K m}^{-1}$
Advection of potential temperature	$A_\theta$	$6.40 \times 10^{-4}$	$\text{K s}^{-1}$
Initial BL specific humidity	$\langle q \rangle$	16.8 <sup>c</sup>	$\text{g kg}^{-1}$
Initial FT specific humidity	$q_{FT}$	12.8	$\text{g kg}^{-1}$
Specific humidity lapse rate FT	$\gamma_q$	-0.004	$\text{g kg}^{-1} \text{m}^{-1}$
Advection of specific humidity	$A_q$	$1.50 \times 10^{-4}$	$\text{g kg}^{-1} \text{s}^{-1}$

<sup>a</sup> Data from ceilometer measurement at the SEARCH site.<sup>b</sup> The peak values of the heat fluxes are obtained from the AABC tower.  $t$  is the elapsed time since the start of the simulation and  $t_d$  is the time difference between the start and end of the simulation period (06:00–16:30 CST).<sup>c</sup> Data from the AABC flux tower.

- [Title Page](#)
- [Abstract](#) | [Introduction](#)
- [Conclusions](#) | [References](#)
- [Tables](#) | [Figures](#)
- [◀](#) | [▶](#)
- [◀](#) | [▶](#)
- [Back](#) | [Close](#)
- [Full Screen / Esc](#)
- [Printer-friendly Version](#)
- [Interactive Discussion](#)



<a href="#">Title Page</a>	
<a href="#">Abstract</a>	<a href="#">Introduction</a>
<a href="#">Conclusions</a>	<a href="#">References</a>
<a href="#">Tables</a>	<a href="#">Figures</a>
<a href="#">◀</a>	<a href="#">▶</a>
<a href="#">◀</a>	<a href="#">▶</a>
<a href="#">Back</a>	<a href="#">Close</a>
<a href="#">Full Screen / Esc</a>	
<a href="#">Printer-friendly Version</a>	
<a href="#">Interactive Discussion</a>	

**Table 3.** The initial mixing ratios of important chemical species in the CBL and FT used in MXLCH.

Species	Mixing ratio in CBL (ppbv)	Mixing ratio in FT (ppbv)	Emission or deposition
O <sub>3</sub>	12.9 <sup>a</sup>	51.0 <sup>c</sup>	2.3 <sup>d</sup>
NO	0.1	0.05 <sup>c</sup>	— <sup>e</sup>
NO <sub>2</sub>	0.8 <sup>a</sup>	0.06 <sup>c</sup>	— <sup>f</sup>
OH	0	0	— <sup>g</sup>
HO <sub>2</sub>	0	0	— <sup>g</sup>
C <sub>5</sub> H <sub>8</sub>	0.6 <sup>b</sup>	0.0	1.0sin( $\pi t/t_d$ ) <sup>g</sup>
MVK	0.3 <sup>b</sup>	0.3 <sup>b</sup>	2.4 <sup>d</sup>
MACR	0.3 <sup>b</sup>	0.3 <sup>b</sup>	2.4 <sup>d</sup>
ISOPND	0.01 <sup>a</sup>	0	1.5 <sup>h</sup>
ISOPNB	0.01 <sup>a</sup>	0	1.5 <sup>h</sup>
ISOOPOOH	0	0	2.5 <sup>h</sup>
Monoterpenes	1.1 <sup>b</sup>	0.0	0.070sin( $\pi t/t_d$ ) <sup>g</sup>

<sup>a</sup> Data are obtained from the SEARCH site.<sup>b</sup> Data are obtained from the WASP system.<sup>c</sup> Data are obtained from NCAR C-130.<sup>d</sup> Dry deposition velocity (unit, cm s<sup>-1</sup>), values taken from Karl et al. (2010).<sup>e</sup> -5sin( $\pi t/t_d$ ) pptv m s<sup>-1</sup> in reduced scheme, -30sin( $\pi t/t_d$ ) pptv m s<sup>-1</sup> in complex scheme.  $t$  is the elapsed time since the start of the simulation and  $t_d$  is the time difference between the start and end of the flux period (06:00–08:00 CST).<sup>f</sup> 5sin( $\pi t/t_d$ ) pptv m s<sup>-1</sup> in reduced scheme, 30sin( $\pi t/t_d$ ) pptv m s<sup>-1</sup> in complex scheme.  $t$  and  $t_d$  are the same as above.<sup>g</sup> The peak values of the BVOCs fluxes are obtained from the AABC tower.  $t$  and  $t_d$  are the same as above.<sup>h</sup> Dry deposition velocity (unit, cm s<sup>-1</sup>), values taken from Nguyen et al. (2015).

**Table 4.** The reduced chemistry scheme used in MXLCH. Product compounds shown in parenthesis (e.g.,  $(O_2)$ ) indicate not included in the model solution.

Number	Reaction	Reaction rate
R01	$O_3 + h\nu \rightarrow O(^1D) + (O_2)$	$3.03 \times 10^{-4} \exp(-1.96/\cos(x))$
R02	$O(^1D) + H_2O \rightarrow 2OH$	$1.63 \times 10^{-10} \exp(60T^{-1})$
R03	$O(^1D) + N_2 \rightarrow O_3$	$2.15 \times 10^{-11} \exp(110T^{-1})$
R04	$O(^1D) + O_2 \rightarrow O_3$	$3.30 \times 10^{-11} \exp(55T^{-1})$
R05	$NO_2 + h\nu \rightarrow NO + O_3$	$1.71 \times 10^{-2} \exp(-0.55/\cos(x))$
R06	$CH_2O + h\nu \rightarrow HO_2$	$1.94 \times 10^{-4} \exp(-0.82/\cos(x))$
R07	$OH + CO \rightarrow HO_2 + (CO_2)$	$2.40 \times 10^{-13}$
R08	$OH + CH_4 \rightarrow CH_3O_2$	$2.45 \times 10^{-12} \exp(-1775T^{-1})$
R09	$OH + C_5H_8 \rightarrow HO C_5H_8OO$	$3.10 \times 10^{-11} \exp(350T^{-1})$
R10	$OH + [MVK+MACR] \rightarrow HO_2 + CH_2O$	$2.40 \times 10^{-11}$
R11	$OH + HO_2 \rightarrow H_2O + (O_2)$	$4.80 \times 10^{-11} \exp(250T^{-1})$
R12	$OH + H_2O_2 \rightarrow H_2O + HO_2$	$2.90 \times 10^{-12} \exp(-160T^{-1})$
R13	$HO_2 + NO \rightarrow OH + NO_2$	$3.50 \times 10^{-12} \exp(250T^{-1})$
R14	$CH_3O_2 + NO \rightarrow HO_2 + NO_2 + CH_2O$	$2.80 \times 10^{-12} \exp(300T^{-1})$
R15	$HO C_5H_8OO + NO \rightarrow HO_2 + NO_2 + 0.7[MVK+MACR] + CH_2O$	$1.00 \times 10^{-11}$
R16	$OH + CH_2O \rightarrow HO_2$	$5.50 \times 10^{-12} \exp(125T^{-1})$
R17	$2HO_2 \rightarrow H_2O_2 + (O_2)$	a
R18	$CH_3O_2 + HO_2 \rightarrow PRODUCT$	$4.10 \times 10^{-13} \exp(750T^{-1})$
R19	$HO C_5H_8OO + HO_2 \rightarrow 0.8OH + PRODUCT$	$1.50 \times 10^{-11} \exp(750T^{-1})$
R20	$OH + NO_2 \rightarrow HNO_3$	$3.50 \times 10^{-12} \exp(340T^{-1})$
R21	$NO + O_3 \rightarrow NO_2 + (O_2)$	$3.00 \times 10^{-12} \exp(-1500T^{-1})$
R22	$NO + NO_3 \rightarrow 2NO_2$	$1.80 \times 10^{-11} \exp(110T^{-1})$
R23	$NO_2 + O_3 \rightarrow NO_3 + (O_2)$	b
R24	$NO_2 + NO_3 \rightarrow N_2O_5$	c
R25	$N_2O_5 \rightarrow NO_3 + NO_2$	$1.30 \times 10^{-2} \exp(-3.5T^{-1})$
R26	$N_2O_5 + H_2O \rightarrow 2HNO_3$	$2.50 \times 10^{-22}$
R27	$N_2O_5 + 2H_2O \rightarrow 2HNO_3 + H_2O$	$1.80 \times 10^{-39}$
R28	$HO_2 + O_3 \rightarrow OH + 2(O_2)$	$2.03 \times 10^{-16}(T 300^{-1})^{4.57} \exp(693T^{-1})$
R29	$C_{10}H_{16} + O_3 \rightarrow PRODUCT$	$5.00 \times 10^{-16} \exp(-530T^{-1})$
R30	$C_{10}H_{16} + OH \rightarrow PRODUCT$	$1.21 \times 10^{-11} \exp(436T^{-1})$
R31	$OH + O_3 \rightarrow HO_2 + (O_2)$	$1.30 \times 10^{-12} \exp(-956T^{-1})$

$$^a k = (k_1 + k_2)/k_3; k_1 = 2.21 \times 10^{-13} \exp(600T^{-1}); k_2 = 1.91 \times 10^{-33} \exp(980T^{-1})c_{air}; k_3 = 1 + 1.4 \times 10^{-21} \exp(2200T^{-1})c_{H_2O}.$$

$$^b k = 0.35 \times (k_0 \times k_{int})/(k_0 + k_{int}); k_0 = 3.61 \times 10^{-30}(T 300^{-1})^{-4.1}c_{N_2}; k_{int} = 1.91 \times 10^{-12}(T 300^{-1})^{0.2}.$$

$$^c k = 0.35 \times (k_0 \times k_{int})/(k_0 + k_{int}); k_0 = 1.31 \times 10^{-3}(T 300^{-1})^{-3.5} \exp(-1100T^{-1}); k_{int} = 9.71 \times 10^{14}(T 300^{-1}) \times \exp(-11080T^{-1}).$$

## Isoprene photo-oxidation in the Southeast US

L. Su et al.

Title Page

Abstract

Introduction

Conclusions

References

Tables

Figures



Full Screen / Esc

Printer-friendly Version

Interactive Discussion



**Figure 1.** Schematic of the observations and various processes simulated in the mixed-layer model in this study.

**Figure 2.** Location of the two ground-based sampling sites and typical flight tracks of Long-EZ aircraft. The left panel shows the locations of the SEARCH site (upper red rectangular area) and the AABC site (lower red rectangular area). The two panels on the right side show the typical flight tracks carried out on 12 June over the two sites. The solid red square and solid red triangle indicate the location of the sampling towers at the SEARCH site and the AABC site, respectively. The GPS altitude of both flight tracks are color coded and indicated by the legend on the right. The maps were obtained from Google Earth.

**Isoprene  
photo-oxidation in  
the Southeast US**

L. Su et al.

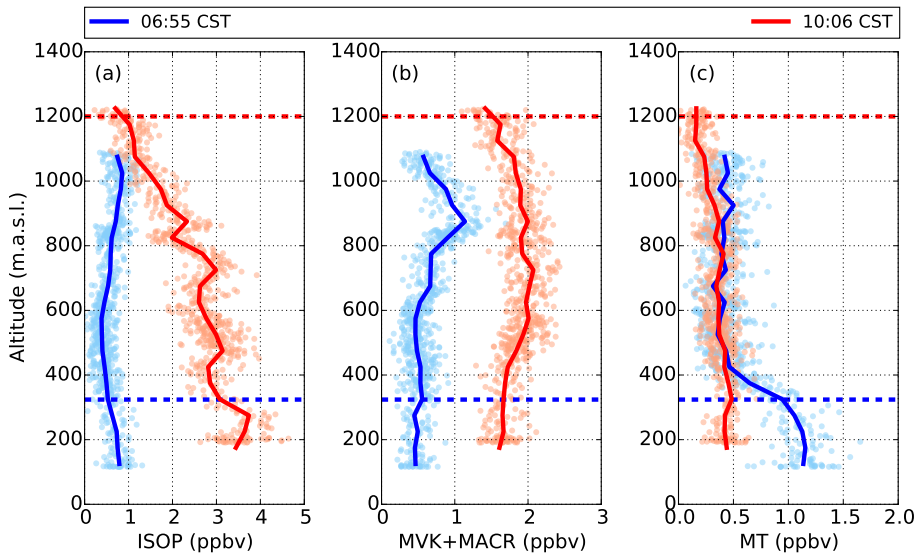


**Figure 3.** Vertical profiles of VOC species collected using the WASP system. The blue and red colors indicate data collected on 1 June 2013 (at 06:55 CST, over the AABC site) and on 11 June 2013 (at 10:06 CST, over the SEARCH site), respectively. The dots represent original data points from the WASP system. The solid lines represent averaged data from the corresponding original data points within each 50 m altitude intervals. The dashed lines represent the estimated boundary layer height from ceilometer measurements (cf. Fig. 4c). The y axis represents GPS altitude in unit of meters above mean sea level (m.a.s.l.). The elevation of the sampling sites is ~ 67 m.a.s.l.

- [Title Page](#)
- [Abstract](#) [Introduction](#)
- [Conclusions](#) [References](#)
- [Tables](#) [Figures](#)
- [◀](#) [▶](#)
- [◀](#) [▶](#)
- [Back](#) [Close](#)
- [Full Screen / Esc](#)
- [Printer-friendly Version](#)
- [Interactive Discussion](#)



**Isoprene  
photo-oxidation in  
the Southeast US**

L. Su et al.

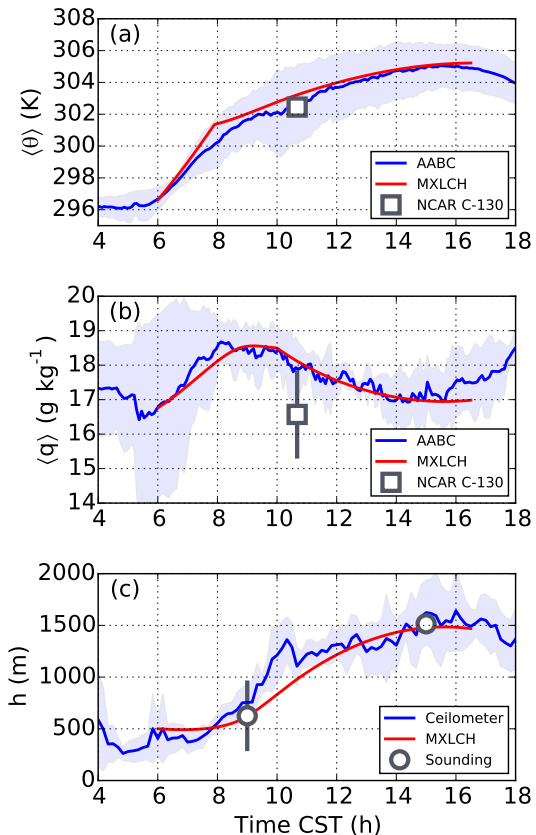


**Figure 4.** Diurnal evolution of **(a)** mixed layer potential temperature ( $\langle \theta \rangle$ ), **(b)** mixed layer specific humidity ( $\langle q \rangle$ ), and **(c)** boundary layer height ( $h$ ). The solid blue lines indicate ground-based observations which are averaged over the low cloud cover days. The shaded areas and error bars indicate 1 standard deviation of the corresponding observations. The solid red lines indicate data from MXLCH outputs.

## Isoprene photo-oxidation in the Southeast US

L. Su et al.

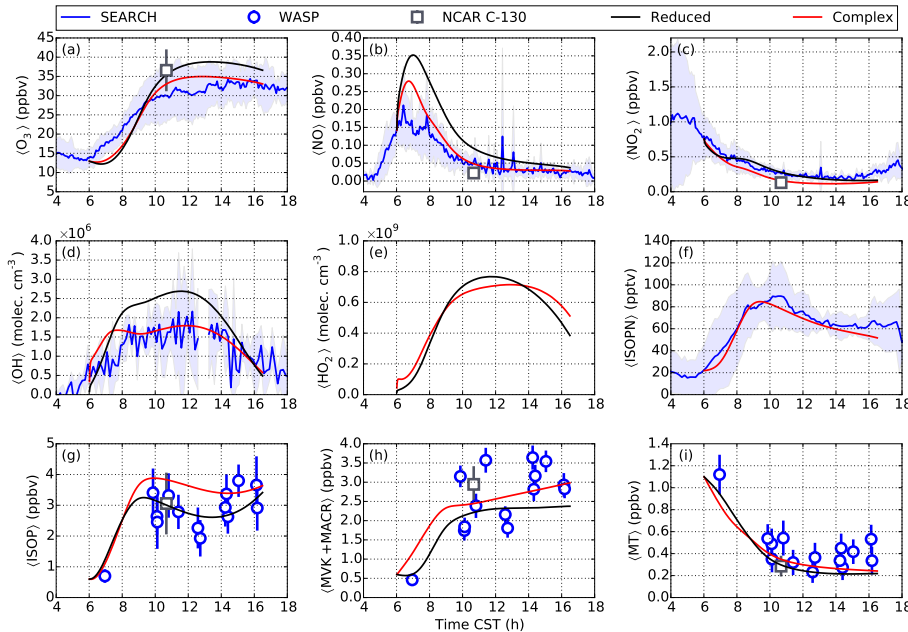


**Figure 5.** Diurnal variation of (a)  $O_3$ , (b) NO, (c)  $NO_2$ , (d) OH, (e)  $HO_2$ , (f) ISOPN, (g) isoprene, (h) MVK+MACR, and (i) monoterpenes. The solid blue line and corresponding shaded light blue area indicate the averaged value and 1 standard deviation from the observation at the SEARCH site. The solid blue circle and corresponding error bar indicate averaged value and 1 standard deviation of VOC mixing ratios within the boundary layer from each RF of the WASP system. The solid black square and corresponding error bar indicate averaged value and 1 standard deviation of chemical species within the boundary layer from RF of the NCAR C-130 aircraft. The solid black and red lines indicate the output from MXLCH model simulation with reduced and complex chemistry schemes, respectively.

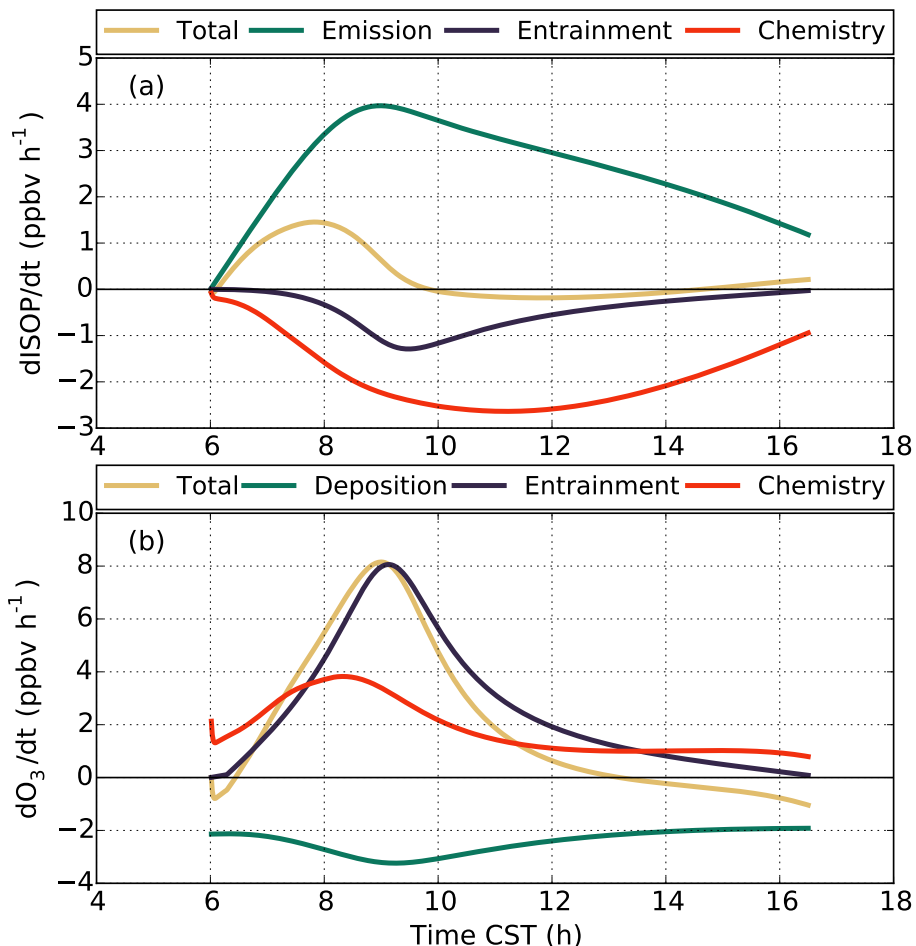


**Figure 6.** Contribution of dynamics and chemistry to the budgets of (a) isoprene, (b) ozone.

# Isoprene photo-oxidation in the Southeast US

L. Su et al.

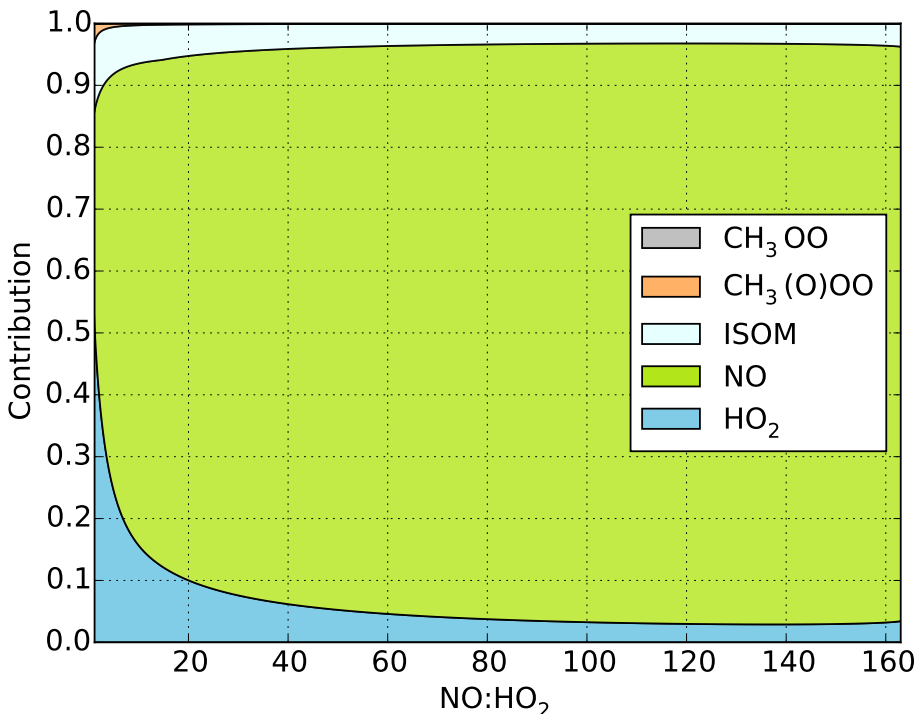


**Figure 7.** Relative contributions of different reaction pathways to the fate of ISOPOO radicals under different  $\text{NO} : \text{HO}_2$  from the MXLCH complex scheme. ISOM indicates isomerization.

Title Page

## Abstract

Introduction

## Conclusion

## References

Table

## Figures

7

1

Bac

**Close**

Full Screen / Esc

[Printer-friendly Version](#)

## Interactive Discussion



# Isoprene photo-oxidation in the Southeast US

L. Su et al.

Title Page

Abstract

tract | Introduction

visions

usions References

les

les | Figures

1

© 2019 Pearson Education, Inc.

2

www.ijerpi.org | 10

2

1

www.nature.com/scientificreports/

© 2013 Pearson Education, Inc.

elter-friendly version

## Interactive Discussion

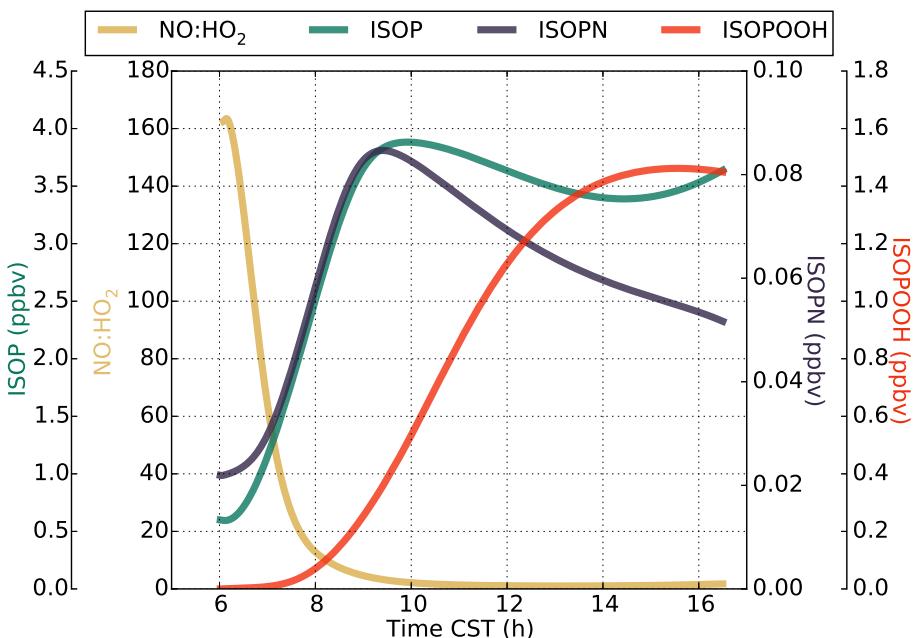


**Figure 8.** Diurnal evolutions of isoprene nitrates (ISOPN), isoprene hydroxy hydroperoxides (ISOPOOH), isoprene (ISOP), and NO : HO<sub>2</sub> from the MXLCH complex scheme.